

Projection in negative norms and the regularization of rough linear functionals

F. Millar^a · I. Muga^a · S. Rojas^a · K.G. Van der Zee^b

Received: date / Accepted: date

Abstract In order to construct regularizations of continuous linear functionals acting on Sobolev spaces such as $W_0^{1,q}(\Omega)$, where $1 < q < \infty$ and Ω is a Lipschitz domain, we propose a projection method in negative Sobolev spaces $W^{-1,p}(\Omega)$, p being the conjugate exponent satisfying $p^{-1} + q^{-1} = 1$. Our method is particularly useful when one is dealing with a rough (irregular) functional that is a member of $W^{-1,p}(\Omega)$, though not of $L^1(\Omega)$, but one strives for a regular approximation in $L^1(\Omega)$. We focus on projections onto discrete finite element spaces G_n , and consider both discontinuous as well as continuous piecewise-polynomial approximations.

While the proposed method aims to compute the best approximation as measured in the negative (dual) norm, for practical reasons, we will employ a computable, discrete dual norm that supremizes over a discrete subspace V_m . We show that this idea leads to a fully discrete method given by a mixed problem on $V_m \times G_n$. We propose a discontinuous as well as a continuous lowest-order pair, prove that they are compatible, and therefore obtain quasi-optimally convergent methods.

We present numerical experiments that compute finite element approximations to Dirac delta's and line sources. We also present adaptively generate meshes, obtained from an error representation that comes with the method. Finally, we show how the presented projection method can be used to efficiently compute numerical approximations to partial differential equations with rough data.

1 Introduction

In the approximation of solutions to partial differential equations (PDEs), the right-hand side data (e.g., sources) may not necessarily be representable by the action of an L^2 (or, more generally, L^1) function. We will refer to such functionals as being *rough*, or irregular. For instance, rough linear functionals f acting on functions $v : \Omega \rightarrow \mathbb{R}$, with Ω being a d -dimensional Lipschitz domain, include:

^a Instituto de Matemáticas, Pontificia Universidad Católica de Valparaíso, Chile.

^b School of Mathematical Sciences, University of Nottingham, UK.

(i) Singular actions over derivatives:

$$f(v) := \int_{\Omega} \vec{F} \cdot \nabla v. \quad (\text{where } \vec{F} \text{ has some kind of singularity in } \Omega)$$

(ii) Point sources, defined by a Dirac delta $\delta_{(\cdot)}$ distribution or derivatives of it:

$$f(v) := \langle \delta_{x_0}, v \rangle = v(x_0). \quad (\text{for a given } x_0 \in \Omega)$$

(iii) Line sources with density ψ :

$$f(v) := \int_C \psi v. \quad (\text{for a given a contour } C \subset \overline{\Omega})$$

There are several numerical complications when dealing with rough functionals:

- PDEs with rough data have low-regular solutions, which imply low convergence rates with quasi-uniform discretizations (e.g., finite element discretizations using uniformly-refined meshes);
- Adaptive methods may recover optimal convergence rates (in terms of number of degrees of freedom), however, standard refinement indicators may not be valid or may be impractical (because of the data being rough, hence does not have an L^2 norm);
- Software packages may not support the implementation of rough functionals, but only facilitate standard domain integrals, i.e.,

$$f(v) = \int_{\Omega} \phi v, \quad (\text{for a given } \phi : \Omega \rightarrow \mathbb{R})$$

to allow for an efficient quadrature treatment.

A natural idea to overcome these complications is to employ *regularizations* of the rough functional f ; cf. Hosseini et al. [39]. To explain the effect of regularizations of f on errors, consider the abstract linear problem

$$\mathcal{L}u = f \quad \text{in } V^*$$

defined by a continuous and bounded below operator $\mathcal{L} : U \mapsto V^*$, where U and V are (trial and test) Banach spaces¹, and V^* is the dual space of V . Let $f_n \in V^*$ be a regularization of f and let

$$u_n := \mathcal{L}^{-1} f_n$$

be the exact solution for the regularized problem. If $u_{n,h}$ is a numerical approximation to u_n , then by the triangular inequality:

$$\|u - u_{n,h}\|_U \leq \underbrace{\|u - u_n\|_U}_{\text{Regularization error}} + \underbrace{\|u_n - u_{n,h}\|_U}_{\text{Discretization error}}. \quad (1)$$

¹ This is the situation commonly encountered in variational formulations of PDEs, where $b(u, v) = \langle f, v \rangle_{V^*, V}$ and $\mathcal{L}u := b(u, \cdot)$, for a given continuous bilinear form $b : U \times V \rightarrow \mathbb{R}$.

Assuming that the *discretization error* can be controlled efficiently by standard adaptive procedures, the error estimate (1) will be dominated by the *regularization error*, for which we know that

$$\|u - u_n\|_U \leq \gamma^{-1} \|f - f_n\|_{V^*}, \quad (2)$$

where $\gamma > 0$ is the stability (inf-sup) constant of the operator \mathcal{L} . Thus, the focus of attention now is on how to control the error $\|f - f_n\|_{V^*}$ (if possible, up to a given accuracy). Notice that the data regularization error, $f - f_n$, is naturally measured in the dual norm $\|\cdot\|_{V^*}$, which in typical situations corresponds to a negative Sobolev space norm.

The main purpose of this paper is to propose and analyse a general methodology, in the wide context of Banach spaces, to construct a robust projection of f into a finite dimensional subspace $G_n \subset V^*$. The projection $f_n \in G_n$ is constructed to have the desirable qualities of being regular and being a near-best approximation to f (as measured by $\|\cdot\|_{V^*}$). We focus on projections onto discrete finite element spaces $G_n \subset L^\infty(\Omega)$, and consider both discontinuous as well as continuous piecewise-polynomial approximations. Such projections f_n allow for exact integration of the usual finite element domain integrals $\int_\Omega f_n v$ via quadrature.²

Our methodology builds upon the discrete-dual minimal-residual (DDMRes) method in Banach spaces [42, 44]. The principle behind this method is residual minimization in dual norms, the idea of which can be traced back to Discontinuous Petrov–Galerkin (DPG) methods [25]. Applied to the current setting, the problem is indeed to minimize $\|f - g_n\|_{V^*}$ amongst $g_n \in G_n$, which is nothing but a projection problem in dual (negative) norms. For computability reasons, the dual norm is replaced by a discrete dual norm $\|f - g_n\|_{(V_m)^*}$, where V_m is a suitable discrete subspace of V .

The main contributions of our work are as follows. By means of a mathematical object known as the *duality map* (see Section 2.3), we prove the equivalence between the negative-norm projection problem and a monotone-mixed formulation that is suitable for finite element discretizations (Theorem 4). The discrete (computable) counterpart of this monotone-mixed formulation is proved to be well-posed and lead to quasi-optimal convergence (Theorem 6) under a Fortin compatibility condition on the trial-test pairing G_n - V_m (cf. [37]), which in turn, is equivalent to a discrete inf-sup compatibility condition (see, e.g., [31]). Thus, the discrete method delivers projections $\tilde{f}_n \in G_n$ that are near-best to $f \in V^*$, hence satisfy:

$$\|f - \tilde{f}_n\|_{V^*} \leq C \inf_{g_n \in G_n} \|f - g_n\|_{V^*}.$$

Moreover, the discrete method is shown to be equivalent to a best-approximation problem in a discrete-dual norm (Theorem 5).

We furthermore propose lowest-order pairs of finite element spaces and prove their Fortin compatibility. The $\mathbb{P}_0/(\mathbb{P}_1 + \text{bubble})$ compatible pair (Proposition 8) uses

² Note also that when using piecewise polynomial f_n , conveniently, data oscillation may vanish in standard a posteriori error estimates, as used in adaptive FEM; see, e.g., [20, 19].

a discontinuous piecewise-constant finite element space for G_n and continuous linears enriched with element bubbles for V_m . The $\mathbb{P}_1 f / \mathbb{P}_2$ compatible pair (Proposition 9) uses a continuous piecewise-linear finite element space for G_n and continuous quadratics for V_m . We perform numerical experiments (Section 5) with these pairs that confirm their stability. We also test numerically the pair consisting of piecewise-constants for G_n and the lowest-order *nonconforming* Crouzeix-Raviart space for V_m (Section 5.2), whose compatibility is an open problem.

The discrete method also has a built-in residual representative. We show that this leads to a natural a posteriori error estimator, which can be localized and employed to conduct adaptive mesh refinements showing outstanding convergence rates (see Section 5). Moreover, we have observed that flatter norms (i.e., $W^{-1,p}(\Omega)$ -norms with exponents p closer to 1) induce a better localization of such mesh refinements.

1.1 Instability when using the L^2 projection

We wish to highlight that a naive L^2 projection for rough functionals may result in unexpected or unwanted results. We illustrate this with a simple 1-D example.

Let $\Omega = (0, 1)$ and consider the rough functional $f \in H^{-1}(0, 1) := (H_0^1(0, 1))^*$ defined by:

$$f(v) := \int_0^1 x^{-\frac{1}{4}} v'(x) dx, \quad \forall v \in H_0^1(0, 1).$$

For a given small parameter $\varepsilon > 0$, we are going to approximate this functional using the one dimensional space generated by the *hat* function:

$$\phi_\varepsilon(x) := \begin{cases} x\varepsilon^{-1} & \text{if } x \in (0, \varepsilon), \\ (1-x)(1-\varepsilon)^{-1} & \text{if } x \in (\varepsilon, 1). \end{cases}$$

If we intend to compute the L^2 -projection of the rough functional $f(\cdot)$ onto the one-dimensional space generated by ϕ_ε we arrive at the problem of finding $\alpha \in \mathbb{R}$ such that:

$$\alpha \|\phi_\varepsilon\|_{L^2(0,1)}^2 = \int_0^1 x^{-\frac{1}{4}} \phi_\varepsilon'(x) dx = \frac{1}{\varepsilon} \int_0^\varepsilon x^{-\frac{1}{4}} dx - \frac{1}{1-\varepsilon} \int_\varepsilon^1 x^{-\frac{1}{4}} dx.$$

Notice that the right hand side of the above equation is of order $\varepsilon^{-1/4}$ and goes to infinity as $\varepsilon \rightarrow 0$. However, the L^2 -norm of ϕ_ε equals $\sqrt{3}/3$, irrespective of ε . Thus, the L^2 -projection $\alpha\phi_\varepsilon$ diverges as $\varepsilon \rightarrow 0$.

On another hand, we have computed the exact H^{-1} -projection of f onto the one-dimensional span of ϕ_ε , together with a discrete H^{-1} -projection onto the same one-dimensional space, but using our proposed methodology with a \mathbb{P}_2 test space setting (see Section 4.2 for further details). The L^2 -norm of these best approximations are depicted in Figure 1, and compared with the divergent L^2 -projection. The H^{-1} projections show stable behaviors as $\varepsilon \rightarrow 0^+$.

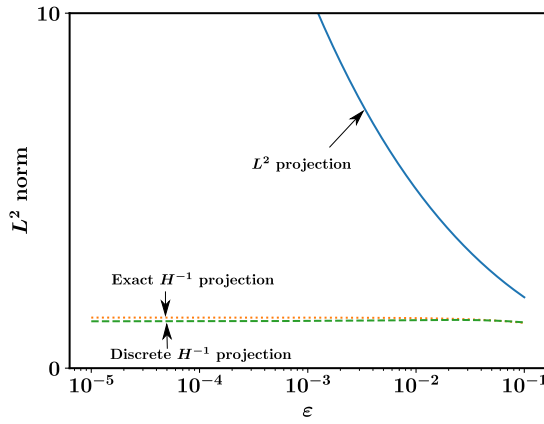


Fig. 1 L^2 norm of exact and discrete H^{-1} -projections of a rough functional over the one-dimensional space generated by ϕ_ε , for several small values of $\varepsilon > 0$.

1.2 Related literature

Solutions of second-order PDEs driven by rough sources may become singular. Indeed, it is well-known that the free-space solution of the Poisson problem:

$$-\Delta u = \delta_{x_0}, \quad (3)$$

exhibits a log-type singularity in two-dimensions; and a singular behavior of the type $1/\text{dist}(x, x_0)$ in three-dimensions. In fact, for dimensions $d \geq 2$, the solution of (3) does not reach the Hilbert space $H^1(\Omega)$, mainly because the Dirac delta distribution is not in the dual space of $H^1(\Omega)$. Nevertheless, a regularized version of δ_{x_0} (e.g., an approximation represented by an $L^2(\Omega)$ function) would produce a regular solution of the Poisson problem, for which standard adaptive procedures work efficiently (see, e.g., [27, 52, 41, 12, 49, 48]).

Rough or singular data has taken the attention of finite element analysts since the early works of Babuška [9] and Scott [46], where they analyzed *a priori* error estimates and convergence rates for the Galerkin method applied to elliptic problems with singular source data, in the context of fractional Sobolev (Hilbert) norms H^s . In particular, Scott uses explicit regularizations of the delta distribution to estimate the regularization error. Later on, Eriksson [28] showed optimal convergence order in L^1 and $W^{1,1}$ norms, depending on adequate graded meshes adapted for Dirac delta right-hand sides. In a more general Banach-space setting, Casado-Diaz et al. [18] proved the $W_0^{1,p}$ -convergence and error estimates, for $1 \leq p \leq d/(d-1)$, of piecewise linear polynomials approximating the solution of second order elliptic equations in divergence form with right-hand sides in L^1 (cf. Example 1). They also showed $W_0^{1,p}$ -weak convergence when the right-hand side is a general Radon measure (see also [22, 34]).

From the point of view of *a posteriori* error analysis and adaptive finite element methods, rough right-hand sides in H^{-1} has been considered in early works of Nochetto [45] and Stevenson [49, 48]. The latter mainly rely on the approximability of

H^{-1} functionals by piecewise constants functions. A different approach was taken by Cohen et al. [23], where they provide H^{-1} -convergent algorithms directly using indicators based on local H^{-1} norms. In the same spirit, Blechta et al. [13] study the localization in negative norms $W^{-1,p}$ for *a posteriori* error estimates purposes.

Point sources have attracted major attention throughout the existing Literature. Recall that the exact solutions to these problems are commonly not encountered in standard Hilbert spaces like H^1 . To overcome this drawback, we can distinguish adaptive approaches based on *a posteriori* error estimates in the natural $W^{1,p}$ -setting of these equations (see, e.g., [7,8,5,33]); or approaches based on error estimates in fractional (and Hilbert) Sobolev norms H^s (see, e.g., [35]); or approaches based on weighted Muckenhoupt norms (see, e.g., [2,3,4]). On another hand, we can also find methods based on mesh-grading techniques (see, e.g., [6,24]), and methods based on regularization techniques (see, e.g., [53,51,50,11,39,10,38,32]). Many of the former results also apply for line sources (see, e.g., [24,36,40]).

1.3 Outline

The outline of the paper is as follows. In Section 2, we present the preliminary concepts related to best approximation in Banach spaces and the functional analysis tools to be required. Section 3 introduces the abstract regularization methodology of rough functionals as a best approximation problem (or projection problem) in dual norms, which in turns is equivalent to a monotone (non-linear) mixed method that can be approached numerically. We provide discrete well-posedness, stability, and *a priori* error analysis in Theorem 6. Additionally, *a posteriori* error analysis can be found in Theorem 7. In Section 4, we provide two trial/test compatible pairs for which our methodology is proved to be well-posed and stable, namely, the $\mathbb{P}_0/\mathbb{P}_1$ +bubbles compatible pair, and the $\mathbb{P}_1/\mathbb{P}_2$ compatible pair. Due to their technicality, the proofs of these last results have been shifted to Appendix A and B, respectively. In Section 5, we perform numerical experiment with point sources and line sources, together with solutions of PDEs with regularized source. Finally, we outline some conclusions and future work in Section 6.

2 Preliminaries

2.1 Functional spaces and rough linear functionals

Let $(X, \|\cdot\|_X)$ be a normed space. The dual space of X (i.e., all the real valued continuous linear functionals defined on X) will be denoted by X^* . The action of $F \in X^*$ over elements $x \in X$ will be denoted by a duality pairing between X^* and X , i.e.,

$$\langle F, x \rangle_{X^*, X} := F(x).$$

The norm of the dual space X^* is defined by

$$\|\cdot\|_{X^*} := \sup_{x \in X} \frac{\langle \cdot, x \rangle_{X^*, X}}{\|x\|_X}. \quad (4)$$

Let $d \in \mathbb{N}$ denote a spatial dimension and let $\Omega \subset \mathbb{R}^d$ be a bounded Lipschitz domain. Consider the standard Lebesgue space $L^q(\Omega)$ (for $q \geq 1$) and the Sobolev spaces:

$$W^{1,q}(\Omega) := \{v \in L^q(\Omega); \nabla v \in [L^q(\Omega)]^d\}, \quad (5)$$

where the q^{th} -power of the norm is defined by

$$\|v\|_{W^{1,q}(\Omega)}^q := \|v\|_{L^q(\Omega)}^q + \|\nabla v\|_{L^q(\Omega)}^q.$$

Let $\mathcal{C}_0^\infty(\Omega)$ be the space of smooth functions with compact support on Ω , and consider the subspace $W_0^{1,q}(\Omega) \subset W^{1,q}(\Omega)$ defined by:

$$W_0^{1,q}(\Omega) := \overline{\mathcal{C}_0^\infty(\Omega)}^{\|\cdot\|_{W^{1,q}(\Omega)}}.$$

By Poincaré's inequality, it is well-known that $\|\cdot\|_{W_0^{1,q}(\Omega)} := \|\nabla(\cdot)\|_{L^q(\Omega)}$ defines an equivalent norm on $W_0^{1,q}(\Omega)$. The dual of the Sobolev space $W_0^{1,q}(\Omega)$ will be denoted with a negative exponent, i.e.,

$$W^{-1,p}(\Omega) := \left(W_0^{1,q}(\Omega)\right)^*,$$

where $p^{-1} + q^{-1} = 1$. The associated dual norm is given accordingly to (4), in which case we talk about a *negative norm*.

Remark 1. *The reader can refer to [1, 26] for the definition of Sobolev spaces $W^{s,q}(\Omega)$ with higher or even fractional derivatives of order $s > 0$. In general, we will use the terminology negative norm to denote the supremum norm (4) of the dual of a Sobolev space $W^{s,q}(\Omega)$, with $s > 0$.*

The following examples, typify what we understand by irregular and rough linear functionals in negative Sobolev spaces.

Example 1 (Irregular functions). *For $f \in L^r(\Omega)$, with $r \geq 1$, the application $v \mapsto \int_\Omega f v$ defines a continuous linear functional over $L^q(\Omega)$, for any $q \geq r^* := r/(r-1)$. However, it also defines a continuous linear functional over $W^{1,q}(\Omega)$, for a wider spectrum of values of $q \geq 1$. Indeed, one can show that*

$$\left| \int_\Omega f v \right| \leq \|f\|_{L^r(\Omega)} \|v\|_{L^{r^*}(\Omega)} \lesssim \|f\|_{L^r(\Omega)} \|v\|_{W^{1,q}(\Omega)},$$

provided the embedding $W^{1,q}(\Omega) \hookrightarrow L^{r^}(\Omega)$ holds true continuously. This is always the case in one dimension, i.e., for $d = 1$, the embedding holds true continuously for any $q \geq 1$. In higher dimensions extra assumptions are needed. For instance, if $\Omega \subset \mathbb{R}^d$ has the cone property (see [1, Theorem 5.4]), then the embedding holds true continuously for any $q \geq r^* d / (r^* + d)$. For example, if $f \in L^1(\Omega)$, but $f \notin L^{1+\varepsilon}(\Omega)$, for any $\varepsilon > 0$, then $q \geq d$ is needed.*

Example 2 (Actions over derivatives). *Let $g \in [L^r(\Omega)]^d$ with $r \geq 1$. Then the application*

$$v \mapsto \int_\Omega g \cdot \nabla v,$$

defines a continuous linear functional over $W^{1,q}(\Omega)$ for any $q \geq r^ := r/(r-1)$.*

Example 3 (Point sources). Let $\mathcal{C}(\Omega)$ be the space of continuous real-valued functions over Ω . For $x_0 \in \Omega$, the application $v \mapsto v(x_0)$ defines a continuous linear functional over $W^{1,q}(\Omega)$ provided the embedding $W^{1,q}(\Omega) \hookrightarrow \mathcal{C}(\Omega)$ holds true continuously. The usual requirement for that is $q > d$ (see, e.g., Adams [1, Theorem 5.4]). In such a case, this functional is known as the Dirac delta distribution centered at x_0 , and we write

$$\langle \delta_{x_0}, v \rangle_{(W^{1,q})^*, W^{1,q}} := v(x_0), \quad \forall v \in W^{1,q}(\Omega).$$

Example 4 (Line sources). For $d \geq 2$, let $\Gamma \subset \overline{\Omega}$ be a bounded Lipschitz curve, and let $\phi \in L^r(\Gamma)$. For any $q \geq \max\{d-1, r/(r-1)\}$, the linear application

$$v \mapsto \int_{\Gamma} \phi v, \quad (6)$$

defines a continuous linear functional over $W^{1,q}(\Omega)$. Indeed, in such a case we have $v|_{\Gamma} \in W^{1-\frac{d-1}{q}, q}(\Gamma)$. So the integral in (6) is well-defined and the whole process is continuous due to multiple applications of the trace Theorem.

Of course, Example 4 can be extended to *surface sources* in dimensions $d \geq 3$, and so on and so forth.

2.2 Best approximations in Banach spaces

For a given Banach space, the notion of projection into finite-dimensional subspaces is deeply related to the notion of *best approximation*, which is formalized below in the general context of abstract normed spaces.

Definition 1 (Best approximation). Let X be a normed space and consider a finite dimensional subspace $X_n \subset X$. A best approximation to $x \in X$ in the finite dimensional space X_n , is an element $x_n \in X_n$ such that:

$$\|x - x_n\|_X \leq \|x - z_n\|_X, \quad \forall z_n \in X_n.$$

The following geometrical property of normed spaces will be necessary for the uniqueness of a best approximation (the existence of it, is due to the finite dimensionality of X_n ; see Proposition 1 below).

Definition 2 (Strictly convex space). A normed space X is strictly convex, if for all $x_1, x_2 \in X$, such that $x_1 \neq x_2$ and $\|x_1\|_X = \|x_2\|_X = 1$, it holds that:

$$\|\alpha x_1 + (1 - \alpha)x_2\|_X < 1, \quad \forall \alpha \in (0, 1).$$

Remark 2. The Sobolev space $W^{1,q}(\Omega)$ defined in (5) is strictly convex if and only if $1 < q < +\infty$. The same result holds true for the dual space $(W^{1,q}(\Omega))^*$ (see, e.g., [17, 21]).

Proposition 1 (Existence and uniqueness of a best approximation). Let X be a Banach space and $X_n \subset X$ be a finite-dimensional subspace. For any element in X , there exists at least one best approximation of it in X_n . In addition, if X is a strictly convex Banach space (see Definition 2), then such a best approximation is unique. Moreover,

$$\|x_n\|_X \leq 2\|x\|_X. \quad (7)$$

Proof. This is a classical result (see, e.g., [47, section 10.2]). \square

Remark 3. *The estimate in (7) is not sharp in general and can be improved using geometrical constants of the underlying Banach spaces (see [44, section 3]). Indeed, the reader may observe that in the Hilbert-space case, the constant in (7) must be 1, since x_n corresponds to the orthogonal projection of x .*

2.3 Duality maps

The projection method that we are going to propose is based on operators called *duality maps*, which allows to characterize *best approximations* in a computable manner. We present a particular definition of such an operator in the context of strictly convex Banach spaces (cf. [17, 21]).

Definition 3 (Duality Map). *Let X be a normed space and let us assume that its dual space X^* is a strictly convex Banach space. For $s > 1$, the duality map $\mathcal{J}_{s,X} : X \mapsto X^*$ is the (unique) operator satisfying:*

- i. $\langle \mathcal{J}_{s,X}(x), x \rangle_{X^*, X} = \|\mathcal{J}_{s,X}(x)\|_{X^*} \|x\|_X$
- ii. $\|\mathcal{J}_{s,X}(x)\|_{X^*} = \|x\|_X^{s-1}$.

Remark 4. *The existence of the duality map $\mathcal{J}_{s,X}$ given in Definition 3 is guaranteed by the Hahn-Banach extension Theorem; while the uniqueness of it is due to the strict convexity of X^* (see, e.g. [17, 21]).*

The following duality map identity is crucial for the characterization of *best approximations* (see Corollary 1 below).

Proposition 2. *Let X be a Banach space, such that X^* is strictly convex. Let us consider $\phi : X \rightarrow \mathbb{R}$, defined as $\phi(\cdot) = \frac{1}{s} \|\cdot\|_X^s$, with $s > 1$. Then, ϕ is Gâteaux differentiable for all $x \in X$, and we have the following characterization for the duality map:*

$$\mathcal{J}_{s,X}(x) = \nabla \phi(x). \quad (8)$$

Proof. See e.g. [21, chapter 1, section 2]. \square

As a consequence of Proposition 2, we have the following Corollary.

Corollary 1 *Let X be a Banach space such that X^* is strictly convex. Let $X_n \subset X$ be a finite dimensional subspace. If $x_n \in X_n$ is a best approximation of $x \in X$, then by first-order optimality conditions we have:*

$$\langle \mathcal{J}_{s,X}(x - x_n), z_n \rangle_{X^*, X} = \left\langle \nabla \left(\frac{1}{s} \|x - x_n\|_X^s \right), z_n \right\rangle_{X^*, X} = 0, \quad \forall z_n \in X_n.$$

Example 5 (Duality map of $W^{1,q}(\Omega)$). For $s = q > 1$ and $X = W^{1,q}(\Omega)$, we have the following characterization of the duality map $\mathcal{J}_{W^{1,q}} := \mathcal{J}_{s,X}$ (for any $v, w \in W^{1,q}(\Omega)$):

$$\langle \mathcal{J}_{W^{1,q}}(v), w \rangle_{(W^{1,q})^*, W^{1,q}} := \int_{\Omega} |v|^{q-1} \text{sgn}(v) w + \sum_{i=1}^d \int_{\Omega} |\partial_i v|^{q-1} \text{sgn}(\partial_i v) \partial_i w. \quad (9)$$

Observe that the duality map in (9) is a non-linear operator, except for the Hilbert case $q = 2$, where the duality map coincides with the well-known Riesz map.

In general, the duality map of a dual space is difficult to compute in practice because of the supremum norm (4). However, for smooth Banach spaces (i.e., when X and X^* are strictly convex and reflexive) we have the following helpful characterization.

Proposition 3. *If X and X^* are strictly convex and reflexive Banach spaces, then the duality map is a bijection. Moreover, identifying X^{**} with X , the following characterization holds true*

$$\mathcal{J}_{s^*, X^*} = \mathcal{J}_{s, X}^{-1},$$

where $s^* = s/(s-1)$.

Proof. Reflexivity implies surjectivity of duality maps (see [21, chapter II, theorem 3.4]), while strict convexity of X implies injectivity of them (see [21, chapter II, theorem 1.10]).

Let $x^* \in X^*$ and let $x = \mathcal{J}_{s, X}^{-1}(x^*)$. Identifying X^{**} with X , we notice that:

$$\langle x, x^* \rangle_{X^{**}, X^*} = \langle x^*, x \rangle_{X^*, X} = \langle \mathcal{J}_{s, X}(x), x \rangle_{X^*, X} = \|\mathcal{J}_{s, X}(x)\|_{X^*} \|x\|_X = \|x^*\|_{X^*} \|x\|_{X^{**}},$$

which implies that x satisfies the first requirement of Definition 3. Moreover,

$$\|x\|_{X^{**}}^s = \|x\|_X^s = \|x\|_X^{s^*(s-1)} = \|\mathcal{J}_{s, X}(x)\|_{X^*}^{s^*} = \|x^*\|_{X^*}^{s^*},$$

which implies that x satisfies the second requirement of Definition 3. Hence, by uniqueness (see Remark 4), we must have $x = \mathcal{J}_{s^*, X^*}(x^*)$. \square

3 The proposed projection methodology

3.1 Exact projection in dual norms

In this section, we establish a methodology to construct regularizations of functionals belonging to a dual Banach space, as the best-approximation of them over a given finite-dimensional subspace. For that, we show that the best-approximation problem is equivalent to a monotone mixed formulation, where a residual representative is introduced as a new unknown.

Theorem 4. *Assume that V and V^* are strictly convex and reflexive Banach spaces, and let us consider a finite dimensional subspace $G_n \subset V^*$. Let $\mathcal{J}_{s, V} : V \mapsto V^*$ be the duality map of Definition 3. Given $f \in V^*$, the following statements are equivalent:*

i. $f_n \in G_n$ is the unique best approximation satisfying

$$f_n = \operatorname{argmin}_{g_n \in G_n} \|f - g_n\|_{V^*}. \quad (10)$$

ii. For all $s > 1$, there is a unique residual representative $r \in V$, such that $(r, f_n) \in V \times G_n$ satisfy the semi-infinite monotone mixed formulation:

$$\begin{cases} \langle \mathcal{J}_{s,V}(r), v \rangle_{V^*,V} + \langle f_n, v \rangle_{V^*,V} = \langle f, v \rangle_{V^*,V}, & \forall v \in V, \\ \langle g_n, r \rangle_{V^*,V} = 0, & \forall g_n \in G_n. \end{cases} \quad (11)$$

Proof. A general proof is given in [43, Theorem 3.B] for a wider class of boundedly invertible operators $B : U \rightarrow V^*$ (where U is another Banach space), but using the particular choice of duality map $\mathcal{J}_{2,V}$. It is straightforward to accommodate that proof to the case where $U = V^*$, B is the identity operator in V^* , and $\mathcal{J}_{s,V}$ is any duality map fulfilling Definition 3. Indeed, just for illustrating we will give a proof of how (10) implies (11).

Let f_n be the best-approximation satisfying (10), which is guaranteed by Proposition 1. Consider the duality map $\mathcal{J}_{s^*,V^*} : V^* \mapsto V^{**}$, where $s^* = s/(s-1)$. By Corollary 1 and Proposition 3, we have:

$$0 = \langle \mathcal{J}_{s^*,V^*}(f - f_n), g_n \rangle_{V^{**},V^*} = \langle g_n, \mathcal{J}_{s,V}^{-1}(f - f_n) \rangle_{V^*,V}, \quad \forall g_n \in G_n. \quad (12)$$

Defining the variable $r := \mathcal{J}_{s,V}^{-1}(f - f_n) \in V$ and plugging it into eq. (12) we obtain the second equation of the mixed system (11). Moreover, since $\mathcal{J}_{s,V}(r) = f - f_n \in V^*$, we also obtain the first equation of (11). \square

Remark 5. Using the definition of the duality map (see Definition 3), we get the following relation between the residual representative and the best-approximation error:

$$\|f - f_n\|_{V^*} = \|r\|_V^{s-1}, \quad \text{for } s > 1. \quad (13)$$

Notice that the residual representative $r = \mathcal{J}_{s,V}^{-1}(f - f_n)$ depends on the choice of the duality map (i.e., the parameter $s > 1$), while the best-approximation f_n is independent of that choice.

3.2 The fully-discrete practical method

The monotone mixed formulation (11) is still intractable for computational purposes unless V has finite dimension. The standard way to overcome this drawback is to consider a finite dimensional subspace $V_m \subset V$ and try to compute the following fully-discrete mixed problem:

$$\begin{cases} \text{Find } (r_m, \tilde{f}_n) \in V_m \times G_n \text{ such that} \\ \langle \mathcal{J}_{s,V}(r_m), v_m \rangle_{V^*,V} + \langle \tilde{f}_n, v_m \rangle_{V^*,V} = \langle f, v_m \rangle_{V^*,V}, & \forall v_m \in V_m, \\ \langle g_n, r_m \rangle_{V^*,V} = 0, & \forall g_n \in G_n. \end{cases} \quad (14)$$

Observe that we have used the notation \tilde{f}_n to distinguish between the solution of (14) and the solution f_n of the semi-infinite mixed system (11), or equivalently, the best-approximation (10).

Of course, many questions arise now:

- Is also $\tilde{f}_n \in G_n$ a best-approximation to f in some sense?
- Is the fully discrete mixed problem (14) well-posed?
- Is the solution \tilde{f}_n quasi-optimal in the sense that $\|f - \tilde{f}_n\|_{V^*} \lesssim \|f - f_n\|_{V^*}$?
- Is it possible to use $\|r_m\|_V$ as a reliable and efficient error estimate to drive adaptivity?

The answer to these queries will guide the following theorems.

Theorem 5. *Assume that V and V^* are strictly convex and reflexive Banach spaces. Let $f \in V^*$ and consider finite dimensional approximation spaces $G_n \subset V^*$ and $V_m \subset V$. A discrete functional $\tilde{f}_n \in G_n$ solves the fully-discrete mixed system (14) (together with $r_m \in V_m$), if and only if, \tilde{f}_n is a best-approximation to $f \in V^*$ in the following sense:*

$$\tilde{f}_n = \operatorname{argmin}_{g_n \in G_n} \|f - g_n\|_{(V_m)^*}, \quad \text{where } \|\cdot\|_{(V_m)^*} := \sup_{v_m \in V_m} \frac{\langle \cdot, v_m \rangle_{V^*, V}}{\|v_m\|_V}. \quad (15)$$

Proof. See [44, Theorem 4.1]. □

Remark 6. *Observe that the solution of (15) may not be unique, even when $(V_m)^*$ is strictly convex. This is because $\|\cdot\|_{(V_m)^*}$ is indeed a norm in $(V_m)^*$, but it is not a norm in V^* . In particular, two different elements of G_n may have the same action over the elements of V_m . The following Theorem 6 provides a sufficient condition to guarantee the well-posedness of (14), or equivalently (15).*

Theorem 6. *Let V and V^* be strictly convex and reflexive Banach spaces. Assume that the finite dimensional approximation subspaces $G_n \subset V^*$ and $V_m \subset V$ satisfy the existence of a continuous (Fortin) operator $\Pi : V \rightarrow V_m$ such that:*

$$i. \quad \|\Pi v\|_V \leq C_\Pi \|v\|_V, \quad \forall v \in V \text{ and some } C_\Pi > 0. \quad (16)$$

$$ii. \quad \langle g_n, v - \Pi v \rangle_{V^*, V} = 0, \quad \forall g_n \in G_n, \forall v \in V. \quad (17)$$

Then, for any $f \in V^$, there is a unique $(r_m, \tilde{f}_n) \in V_m \times G_n$ solution of problem (14). The solution satisfies the a priori estimates:*

$$\|r_m\|_V^{s-1} \leq \|f\|_{V^*}. \quad \text{and} \quad \|\tilde{f}_n\|_{V^*} \leq 2C_\Pi \|f\|_{V^*}. \quad (18)$$

Moreover, recalling the solution of (10) $f_n \in G_n$, we have the quasi-optimality properties:

$$\|r_m\|_V^{s-1} \leq \inf_{g_n \in G_n} \|f - g_n\|_{V^*} = \|f - f_n\|_{V^*} \quad (19)$$

$$\|f - \tilde{f}_n\|_{V^*} \leq (1 + 2C_\Pi) \inf_{g_n \in G_n} \|f - g_n\|_{V^*} = (1 + 2C_\Pi) \|f - f_n\|_{V^*}. \quad (20)$$

Proof. A general well-posedness proof can be found in [44, Theorem 4.5] (just accommodate it considering the operator B as the identity in V^*). Nevertheless, we will show here how to obtain the estimates (18), (19) and (20), since their proof is slightly different. Indeed, testing the first equation of the fully-discrete mixed problem (14) with $v_m = r_m$, using the orthogonal property of r_m , and the definition of the duality map (see Definition 3), we obtain:

$$\|r_m\|_V^s = \langle f, r_m \rangle_{V^*, V} = \langle f - g_n, r_m \rangle_{V^*, V} \quad \forall g_n \in G_n,$$

which gives the first estimate in (18) and also (19) after using Cauchy-Schwarz's inequality. For the second estimate in (18) observe that:

$$\begin{aligned} \|\tilde{f}_n\|_{V^*} &= \sup_{v \in V} \frac{\langle \tilde{f}_n, v \rangle_{V^*, V}}{\|v\|_V} \leq C_\Pi \sup_{v \in V} \frac{\langle \tilde{f}_n, \Pi v \rangle_{V^*, V}}{\|\Pi v\|_V} && \text{(by (16) and (17))} \\ &\leq C_\Pi \|\tilde{f}_n\|_{(V_m)^*} && \text{(since } \Pi V \subset V_m) \\ &\leq 2C_\Pi \|f\|_{(V_m)^*} && \text{(by (15) and (7))} \\ &\leq 2C_\Pi \|f\|_{V^*}. && \text{(since } V_m \subset V) \end{aligned}$$

Moreover, it is easy to see that the application $P_n : V^* \rightarrow G_n$ such that $P_n(f) := \tilde{f}_n$ defines a projector for which $\|P_n(f)\|_{V^*} \leq 2C_\Pi \|f\|_{V^*}$ and $P_n(f - g_n) = P_n(f) - g_n$, for any $g_n \in G_n$. Hence we have:

$$\|f - \tilde{f}_n\|_{V^*} = \|(I - P_n)f\|_{V^*} = \|(I - P_n)(f - g_n)\|_{V^*} \leq (1 + 2C_\Pi) \|f - g_n\|_{V^*},$$

which proves (20). \square

Remark 7. An operator satisfying (16) and (17) is known as a Fortin operator (see [14]). The existence of such a Fortin operator requires that

$$\dim(G_n) \leq \dim(V_m). \quad (21)$$

Observe that to ensure stability and quasi-optimality, the constant $C_\Pi > 0$ must be uniformly bounded in terms of the discretization parameters $\{n, m\}$ of the underlying discrete spaces G_n and V_m .

Remark 8. The stability constants $2C_\Pi$ in (18) and $(1 + 2C_\Pi)$ in (20) are not sharp in general. They can be improved using geometrical constants of the underlying Banach spaces V and V^* . See [44, section 4.4] for the details.

Remark 9. For finite element discretizations on quasi uniform meshes $\{\mathcal{T}_h\}_{h>0}$, one would expect that the best approximation $\|f - f_n\|_{V^*}$ is bounded by a constant times h^τ , where $\tau > 0$ is limited by the regularity of $f \in V^*$ and the polynomial degree of the finite element space. See Section 5 for examples with $V^* = W^{-1,p}$.

3.3 A posteriori error estimate

In residual minimization methods, it is customary to use the quantity $\|r_m\|_V$ as an error estimate to drive adaptivity procedures. The next Theorem aims to answer the query about if $\|r_m\|_V$, as an a posteriori error estimate, is indeed reliable and efficient.

Theorem 7 (A posteriori error estimator). *Assume the same conditions of Theorem 6. For any $f \in V^*$, the counterpart $r_m \in V_m$ of the unique solution of the discrete problem (14) satisfies:*

$$\|r_m\|_V^{s-1} \leq \|f - \tilde{f}_n\|_{V^*} \leq \text{osc}(f) + C_\Pi \|r_m\|_V^{s-1}, \quad (22)$$

where the oscillation term is defined by

$$\text{osc}(f) := \sup_{v \in V} \frac{\langle f, v - \Pi v \rangle_{V^*, V}}{\|v\|_V}.$$

Proof. The first inequality (from left to right) in (22) is an immediate consequence of (19). For the second inequality observe that:

$$\begin{aligned} \|f - \tilde{f}_n\|_{V^*} &= \sup_{v \in V} \frac{\langle f - \tilde{f}_n, v - \Pi v + \Pi v \rangle_{V^*, V}}{\|v\|_V} && \text{(since } -\Pi v + \Pi v = 0) \\ &\leq \text{osc}(f) + C_\Pi \sup_{v \in V} \frac{\langle f - \tilde{f}_n, \Pi v \rangle_{V^*, V}}{\|\Pi v\|_V} && \text{(by (16) and (17))} \\ &\leq \text{osc}(f) + C_\Pi \sup_{v \in V} \frac{\langle \mathcal{J}_{s, V}(r_m), \Pi v \rangle_{V^*, V}}{\|\Pi v\|_V} && \text{(by (14))} \\ &\leq \text{osc}(f) + C_\Pi \|r_m\|_V^{s-1}, \end{aligned}$$

where the last inequality has been obtained using Cauchy-Schwarz's inequality and Definition 3. \square

Remark 10. *Using property (17) observe that:*

$$\text{osc}(f) = \sup_{v \in V} \frac{\langle f - g_n, v - \Pi v \rangle_{V^*, V}}{\|v\|_V}, \quad \forall g_n \in G_n.$$

Hence, $\text{osc}(f) \leq (1 + C_\Pi) \inf_{g_n \in G_n} \|f - g_n\|_{V^*}$, which combined with (22) and (19) gives another way to prove (20).

4 Compatible pairs

In this section we introduce two practical options of compatible pairs G_n/V_m verifying the requirements of Theorem 6. The functional context is the following. Let us consider a bounded Lipschitz domain $\Omega \subset \mathbb{R}^d$, and $V := W_0^{1, q}(\Omega)$. Let $V^* = W^{-1, p}(\Omega)$ be the dual space of V , where $p = q/(q-1)$, and let $\mathcal{T}_h = \{T_i\}_{i=1}^n \subset \Omega$ be a simplicial partition of disjoint open elements such that $\cup_{i=1}^n \bar{T}_i = \bar{\Omega}$.

4.1 The $\mathbb{P}_0/(\mathbb{P}_1 + \text{bubbles})$ compatible pair

Let

$$\begin{cases} G_n := \text{span}\{\mathcal{G}_1, \dots, \mathcal{G}_n\} \subset V^*, \\ \text{where } \langle \mathcal{G}_i, \phi \rangle_{V^*, V} := \int_{T_i} \phi, \quad \forall \phi \in V, \text{ for each } T_i \in \mathcal{T}_h. \end{cases} \quad (23)$$

The space G_n defined above is an analog of the piecewise constant space \mathbb{P}_0 . However, notice that G_n is a space of functionals or *actions*, instead of space of *functions*. In order to solve the mixed system (14), we need to come up with a discrete test space $V_m \subset V$ satisfying the requirements of Theorem 6. For that, we consider the interior local bubble functions $b_i \in W_0^{1,q}(T_i)$ defined by:

$$b_i(x) = \prod_{j=1}^{d+1} \lambda_j(x), \quad \forall i = 1, \dots, n, \quad (24)$$

where $\{\lambda_j\}$ are the barycentric coordinates of the simplex T_i . The n -dimensional space generated by these bubble functions will be denoted by:

$$\mathbb{B}_n(\mathcal{T}_h) := \left\{ v \in W_0^{1,q}(\Omega) \cap \mathcal{C}(\overline{\Omega}); v|_{T_i} \in \text{span}\{b_i\}, \forall T_i \in \mathcal{T}_h \right\}. \quad (25)$$

Additionally, we consider the piecewise polynomial finite element space

$$\mathbb{P}_1(\mathcal{T}_h) := \left\{ v \in \mathcal{C}(\overline{\Omega}); v|_{T_i} \in \mathbb{P}_1, \forall T_i \in \mathcal{T}_h \right\}. \quad (26)$$

Proposition 8. *Assume that we have a shape-regular family of affine simplicial meshes $\{\mathcal{T}_h\}_{h>0}$. If $V_m \subset V$ is a finite dimensional subspace containing the spaces $\mathbb{B}_n(\mathcal{T}_h)$ and $\mathbb{P}_1(\mathcal{T}_h) \cap W_0^{1,q}(\Omega)$, then V_m and G_n (defined in (23)) satisfy the assumptions of Theorem 6, i.e., there exists a Fortin operator $\Pi : V \mapsto V_m$ verifying (16) and (17), with a mesh-independent constant $C_\Pi > 0$.*

Proof. See Appendix A. □

Remark 11. *An alternative to $\mathbb{B}_n(\mathcal{T}_h)$ can be any n -dimensional space generated by piecewise linear and continuous bubbles supported on each of the elements of \mathcal{T}_h , which somehow is a space of extra h -refinements of $\mathbb{P}_1(\mathcal{T}_h)$.*

Remark 12. *Notice that the following practical piecewise polynomial finite element space contains both $\mathbb{B}_n(\mathcal{T}_h)$ and $\mathbb{P}_1(\mathcal{T}_h) \cap W_0^{1,q}(\Omega)$ spaces:*

$$\mathbb{P}_{d+1}(\mathcal{T}_h) \cap W_0^{1,q}(\Omega) := \left\{ v \in W_0^{1,q}(\Omega) \cap \mathcal{C}(\overline{\Omega}); v|_{T_i} \in \mathbb{P}_{d+1}, \forall T_i \in \mathcal{T}_h \right\}.$$

4.2 The $\mathbb{P}_1/\mathbb{P}_2$ compatible pair

Consider the space $\mathbb{P}_1(\mathcal{T}_h)$ defined in (26) and let $\{\varphi_i\}_{i=1}^{N_v}$ be the set of nodal basis functions spanning $\mathbb{P}_1(\mathcal{T}_h) \cap W_0^{1,p}(\Omega)$, where N_v corresponds to the number of interior vertices associated with \mathcal{T}_h . Let

$$\begin{cases} G_{N_v} := \text{span}\{\mathcal{G}_1, \dots, \mathcal{G}_{N_v}\} \subset V^*, \\ \text{where, } \langle \mathcal{G}_i, \phi \rangle_{V^*, V} := \int_{\Omega} \varphi_i \phi, \quad \forall \phi \in V, \text{ for each } i = 1, \dots, N_v. \end{cases} \quad (27)$$

Moreover, let

$$\mathbb{P}_2(\mathcal{T}_h) := \{v \in \mathcal{C}(\overline{\Omega}); v|_{T_i} \in \mathbb{P}_2, \forall T_i \in \mathcal{T}_h\}. \quad (28)$$

We next introduce the notion of quasi-uniform patches that will be essential in the proof of pair-compatibility.

Definition 1 (Quasi-uniform patches) Let $\{\mathcal{T}_h\}_{h>0}$ be a family of affine simplicial meshes. Let $\{\varphi_i\}_{i=1}^{N_v}$ be the set of nodal basis functions spanning $\mathbb{P}_1(\mathcal{T}_h) \cap W_0^{1,p}(\Omega)$. For each $i = 1, \dots, N_v$, let $P_i := \text{supp } \varphi_i$ be the patch of elements supporting the function φ_i , and let us denote by $h_T > 0$ the diameter of each element $T \subset P_i$. We say that the family $\{\mathcal{T}_h\}_{h>0}$ has quasi-uniform patches, if and only if there exists a mesh-independent constant $c > 0$ such that $h_T \leq ch_{\tilde{T}}$, for any two elements T and \tilde{T} within the patch P_i .

Remark 13. A family $\{\mathcal{T}_h\}_{h>0}$ having quasi-uniform patches may seem restrictive for adaptive mesh refinements, because the condition $h_T \leq ch_{\tilde{T}}$ risk being violated at some level. However, the next Lemma 1 shows that this quasi-uniformity condition is indeed implied by the standard shape-regularity assumption on the meshes.

Lemma 1 If $\{\mathcal{T}_h\}_{h>0}$ is a shape-regular family of affine simplicial meshes, then such a family has quasi-uniform patches (see Definition 1).

Proof. For any patch P in the family of meshes, is enough to show the existence of a mesh independent constant $c > 0$ such that $h_T \leq ch_{\tilde{T}}$, for any two elements $T, \tilde{T} \subset P$. By shape-regularity, we know the existence of a mesh-independent constant $\sigma > 1$ such that:

$$\frac{h_T}{\rho_T} \leq \sigma,$$

for every element $T \subset P$, where ρ_T denotes the diameter of the largest inscribed ball in T .

Let T_i and T_{i+1} be two adjacent elements in P , with diameters h_{T_i} and $h_{T_{i+1}}$ (respectively), and diameters ρ_{T_i} and $\rho_{T_{i+1}}$ of the largest inscribed balls within T_i and T_{i+1} , respectively. Let $e_i := \overline{T_i} \cap \overline{T_{i+1}}$ be the common edge/face between T_i and T_{i+1} . In particular, we have

$$h_{T_{i+1}} \geq |e_i| \geq \rho_{T_i},$$

which, combined with shape-regularity, delivers

$$\frac{h_{T_i}}{h_{T_{i+1}}} \leq \frac{h_{T_i}}{|e_i|} \leq \frac{h_{T_i}}{\rho_{T_i}} \leq \sigma. \quad (29)$$

Shape-regularity also warranties that the angles of any simplex in any mesh are uniformly bounded away from zero (see, e.g., [30, Remark 11.5]). This last implies that there is a uniform maximum number of N elements allowed per patch. Thus, any two elements in a patch P (say, T and \hat{T}), they can be connected by a sequence of adjacent elements $\{T_1, T_2, \dots, T_M\}$, where $T_1 = T$, $T_M = \hat{T}$, T_i is adjacent to T_{i+1} , and $M \leq N$. Hence,

$$\frac{h_T}{h_{\hat{T}}} = \frac{h_{T_1}}{h_{T_M}} = \frac{h_{T_1}}{h_{T_2}} \times \dots \times \frac{h_{T_{M-1}}}{h_{T_M}} \leq \sigma^{N-1},$$

which proves the statement. \square

Finally, the upcoming Proposition 9 establishes the compatibility between the space G_{N_v} with a space $V_m \supseteq \mathbb{P}_2(\mathcal{T}_h) \cap W_0^{1,q}(\Omega)$, under the following assumption.

Assumption 1. Let $\{\mathcal{T}_h\}_{h>0}$ be a shape-regular family of affine simplicial meshes. We assume that for every patch P_i of this family, there is a reference patch $\hat{P}_i \subset \mathbb{R}^d$ of unitary measure, such that every element $\hat{T} \subset \hat{P}_i$ is mapped onto a unique element $T \subset P_i$ through an affine transformation $F_T : \hat{T} \rightarrow T$ of the form $F_T(\hat{x}) = A_T \hat{x} + y_T$, where:

$$|\det A_T| = \frac{|T|}{|\hat{T}|} =: \eta_i, \quad \forall T \subset P_i. \quad (30)$$

The constant η_i will be referred to as the scaling constant of the patch P_i .

Proposition 9. Under the hypothesis of Assumption 1, if $V_m \subset V$ is a finite dimensional subspace containing the space $\mathbb{P}_2(\mathcal{T}_h) \cap W_0^{1,q}(\Omega)$, then V_m and G_{N_v} (defined in (27)) satisfy the assumptions of Theorem 6, i.e., there exists a Fortin operator $\Pi : V \mapsto V_m$ verifying (16) and (17), with a mesh-independent constant $C_\Pi > 0$.

Proof. See Appendix B. \square

5 Applications

5.1 Point sources

As a first application, we consider projections of *Dirac delta* distributions (point sources, see Example 3). It is well known that this distribution does not belong to the Hilbert space $H^{-1}(\Omega) := W_0^{-1,2}(\Omega)$ for dimensions higher or equal than two. In our case, we will consider standard Sobolev spaces³ in which the action of the *Dirac delta* is linear and continuous as it was mentioned in Example 3.

³ i.e., of integer order and without weighted norms.

5.1.1 One dimensional Dirac's Delta projection

Given a partition $\mathcal{T}_h = \{T_i\}_{i=1}^n$ of $\Omega := (0, 1)$, we consider the trial spaces G_n and G_{N_v} defined in (23) and (27), together with the test space $V_m = \mathbb{P}_2(\mathcal{T}_h) \cap W_0^{1,q}(\Omega)$. We compute the mixed system (14), using the duality map related with the norm $\|\cdot\|_{W_0^{1,q}}$, i.e.,

$$\left\langle \mathcal{J}_{W_0^{1,q}}(v), w \right\rangle_{W^{-1,p}, W_0^{1,q}} := \sum_{i=1}^d \int_{\Omega} |\partial_i v|^{q-1} \operatorname{sgn}(\partial_i v) \partial_i w, \quad \forall v, w \in W_0^{1,q}(\Omega).$$

For $p = q = 2$ the duality map is linear. In Fig. 2 we represent graphically the projections obtained for δ_{x_0} in such a case, with $x_0 = 0.5$ and the trial space G_{N_v} . We have considered uniform meshes of $n = 16, 32$ & 64 elements respectively. Results are coherent with what is expected (cf. [39]).

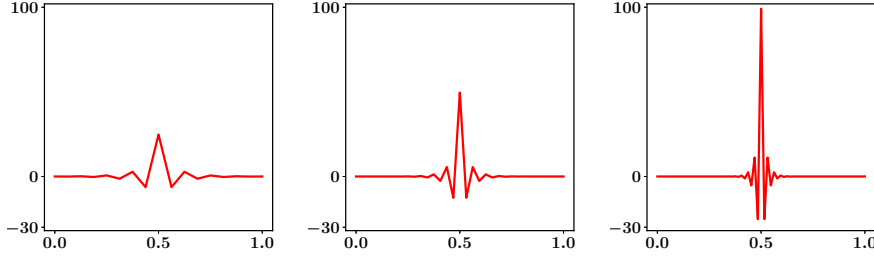


Fig. 2 Sequence of Dirac delta projections over uniform meshes of $n = 16, 32$ & 64 elements.

For $p = \frac{q}{q-1} < 2$, the duality map is nonlinear. Hence, we have resorted to a Newton-Raphson continuation method to solve numerically problem (14). That is, we create a sequence of $(k+1)$ problems with parameters $2 = p_0 > \dots > p_{k-1} > p$, where in each step, problem (14) is solved using the solution of the previous step as initial guess. Using the piecewise constant trial space G_n defined in (23), Fig. 3 depicts the convergence of the residual term $\|r_m\|_V^{q-1}$ compared with total degrees of freedoms (i.e., $\dim(G_n) + \dim(V_m)$) for uniform and adaptive h -refinements, and for several values of $p \in (1, 2)$. Recall that, by Sobolev embeddings in 1D, the Dirac delta action is well-defined in $W_0^{s,q}(\Omega) \subset \mathcal{C}(\Omega)$ whenever $sq > 1$ (see, e.g., [1]). The observed convergence rate for h -refinements is $1/p$, which can be seen as the difference between the regularity exponent $s = 1$ and the critical regularity exponent $s^* = 1/q$ (cf. Remark 9). On the other hand, since the source localizes in only one point, exponential convergence rates are observed for adaptive h -refinements. The marking criteria has been set to refine all the elements showing local error larger than the 50% of the maximum local error.

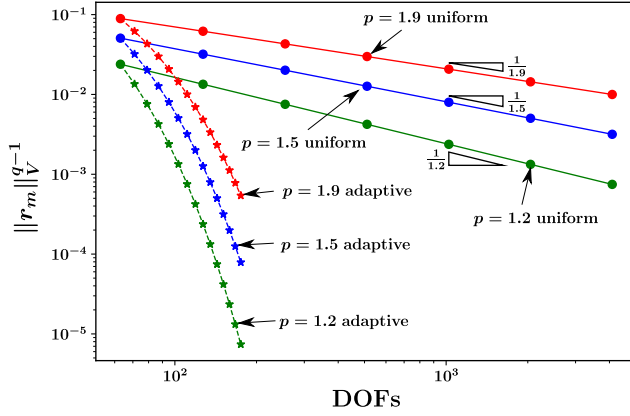


Fig. 3 1D Dirac delta: convergence rates of uniform and adaptive h -refinements for several values of p .

5.1.2 Elliptic ODE with projected Dirac delta source

In this section, we test the performance of the projected Dirac delta acting as the source term of an elliptic ODE. Let $x_0 \in \Omega := (0, 1)$ and $a \geq 0$. Consider the following *exact* problem:

$$\begin{cases} -u'' + a^2 u = \delta_{x_0} & \text{in } \Omega, \\ u(0) = u(1) = 0. \end{cases} \quad (31)$$

It is easy to check that the analytical solution of (31) is:

$$u(x) = \begin{cases} \frac{e^{ax_0} - e^{a(2-x_0)}}{1 - e^{2a}} \frac{\sinh(ax)}{a} & \text{if } 0 \leq x \leq x_0, \\ \frac{\sinh(ax_0)}{a} \frac{e^{ax} - e^{a(2-x)}}{1 - e^{2a}} & \text{if } x_0 \leq x \leq 1. \end{cases} \quad (32)$$

The case $a = 0$ can be obtained performing the limit when $a \rightarrow 0$ in (32), in whose occurrence the solution is piecewise linear and continuous (see Figure 4). Let $\delta_n \in G_n$ be the piecewise constant projection of the Dirac delta, computed using the $\mathbb{P}_0/\mathbb{P}_2$ compatible pair, with $p = q = 2$. Observe that $\delta_n \in L^2(\Omega)$, which induces the following regularized problem:

$$\begin{cases} -u_n'' + a^2 u_n = \delta_n, & \text{in } \Omega, \\ u_n(0) = u_n(1) = 0. \end{cases} \quad (33)$$

In Figure 4, we show the solutions obtained by approximating equation (33) using a Galerkin scheme with conforming $\mathbb{P}_2(\mathcal{T}_h)$ Lagrange finite elements over the same mesh that defines $\delta_n \in G_n$, which in this case corresponds to uniform meshes of $n = 4, 8$ & 32 elements. We have chosen $x_0 = \sqrt{2}/2$ to make sure that x_0 never coincides with a node of the meshes. Moreover, we have considered $a = 0$, which implies that the exact solution of (33) is indeed contained in the discrete space $\mathbb{P}_2(\mathcal{T}_h)$, and thus, there is no discretization error. The convergence rates of the error $\|u - u_n\|_{H_0^1}$ coincide

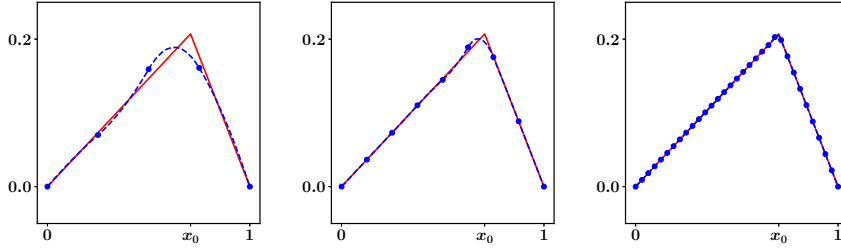


Fig. 4 Regularized solution u_n of problem (33) (dashed line), compared with the exact solution (32) (continuous line), with Dirac delta supported on $x_0 = \sqrt{2}/2$ and $a = 0$. The inputs for u_n have been obtained from projected Dirac deltas onto uniform meshes of $n = 4, 8$ & 32 elements, respectively.

with the convergence rates of $\|\delta_{x_0} - \delta_n\|_{H^{-1}}$ (or, more precisely, with $\|r_m\|_V$), as can be observed from Figure 5.

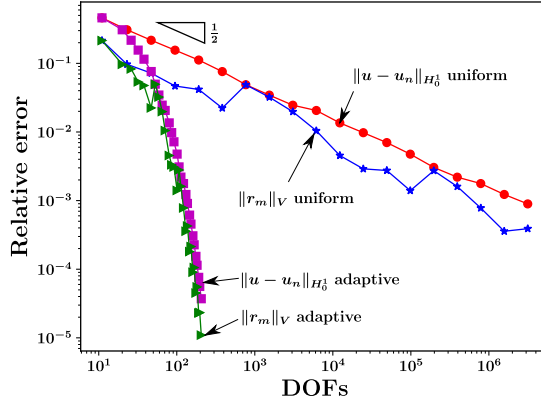


Fig. 5 Convergence rates for the solution of the regularized problem (33).

The next experiment intends to answer the question: *can we approximate the solution of problem (31) up to a given desired precision?* Inspired in the adaptive algorithm proposed by Bonito et al. [15], we propose a two-step adaptive procedure. The first step controls the *regularization error*, while the second step controls the *discretization error*. To fix ideas, let $u_{n,h}$ be the discrete approximation of problem (33) obtained by an adaptive procedure. Observe that:

$$\|u - u_{n,h}\|_{H_0^1} \leq \|u - u_n\|_{H_0^1} + \|u_n - u_{n,h}\|_{H_0^1} \leq \frac{1}{\gamma} \|\delta_{x_0} - \delta_n\|_{H^{-1}} + \|u_n - u_{n,h}\|_{H_0^1},$$

where $\gamma > 0$ is the stability constant of our differential operator ($\gamma = 1$ in this particular example). In the first step, we perform an adaptive projection of the Dirac delta until reaching some prescribed tolerance. This will control the regularization error $\|\delta_{x_0} - \delta_n\|_{H^{-1}}$ and will deliver a projected delta δ_n together with an adapted mesh

$\mathcal{T}_h = \{T_i\}_{i=1}^n$. In the second step, we use the source δ_n obtained in the first step and solve problem (33) adaptively considering \mathcal{T}_h as the initial mesh, until reaching the prescribed tolerance. This will control the discretization error $\|u_n - u_{n,h}\|_{H_0^1}$. The general procedure is depicted in Algorithm 1. In particular, for the second step we have used a standard local *a posteriori* error estimator η_{T_i} , similar to the one used in [15]. Since the RHS δ_n is a piecewise constant function, there is no data oscillation in this case (see, e.g. [41]). Figure 6 (left) depicts the error in H_0^1 semi-norm of the adapted

Algorithm 1 Approximating the solution of a PDE by regularization

```

1: Global tol > 0,  $\alpha_1 \in (0, 1)$ ,  $\alpha_2 \in (0, 1)$ 
2: procedure SOURCE REGULARIZATION ALGORITHM
3:   Input  $\leftarrow$  RHS :=  $\delta_{x_0}$ , mesh :=  $\mathcal{T}_h = \{T_i\}_{i=1}^n$ ,  $q > 1$ 
4:    $(r_m, \delta_n) \leftarrow$  Solve scheme (14)
5:   while tol <  $\|r_m\|_V^{q-1}$  do
6:     if  $\|r_m\|_{V(T_i)}^{q-1} > \alpha_1 \max\{\|r_m\|_{V(T_i)}^{q-1}\}$  then
7:       Refine the element  $T_i$ 
8:     Update mesh  $\mathcal{T}_h$  and go to step 3
9:   return  $\mathcal{T}_h, \delta_n$ 
10: procedure APPROXIMATING THE SOLUTION OF THE REGULARIZED PDE
11:   Input  $\leftarrow$  RHS :=  $\delta_n$ , mesh :=  $\mathcal{T}_h$ 
12:    $u_{n,h} \leftarrow$  Solve the problem (33) by Galerkin method
13:   Compute local a posteriori estimators  $\eta_{T_i}$ 
14:   while tol  $\leq \sqrt{\sum \eta_{T_i}^2}$  do
15:     if  $\eta_{T_i} > \alpha_2 \max\{\eta_{T_i}\}$  then
16:       Refine the element  $T_i$ 
17:     Update mesh  $\mathcal{T}_h$  and go to step 10
18:   return  $\mathcal{T}_h, u_{n,h}$ .

```

discrete solution v/s the chosen tolerance in Algorithm 1. We report here that smaller tolerances would lead to huge condition numbers in the second step of Algorithm 1, making results unreliable. In Figure 6 (right), the final discrete solution, computed using Algorithm 1 with tol = 0.001 and $\alpha_1 = \alpha_2 = 0.5$, is compared with the exact solution. We have set the values $x_0 = \sqrt{2}/2$ and $a = 2$ in (31).

5.1.3 Elliptic PDE with projected Dirac delta source on a L-shape domain.

This section is motivated by the examples shown in [7, 2]. Let $\Omega \subset \mathbb{R}^2$ be the open L-shape domain defined by joining vertices $(0, 0)$, $(0, -1)$, $(1, -1)$, $(1, 1)$, $(-1, 1)$, and $(-1, 0)$. For $x_0 = (\frac{1}{2}, \frac{1}{2}) \in \Omega$, consider the Poisson problem

$$\begin{cases} -\Delta u = \delta_{x_0} & \text{in } \Omega, \\ u = g & \text{on } \partial\Omega, \end{cases} \quad (34)$$

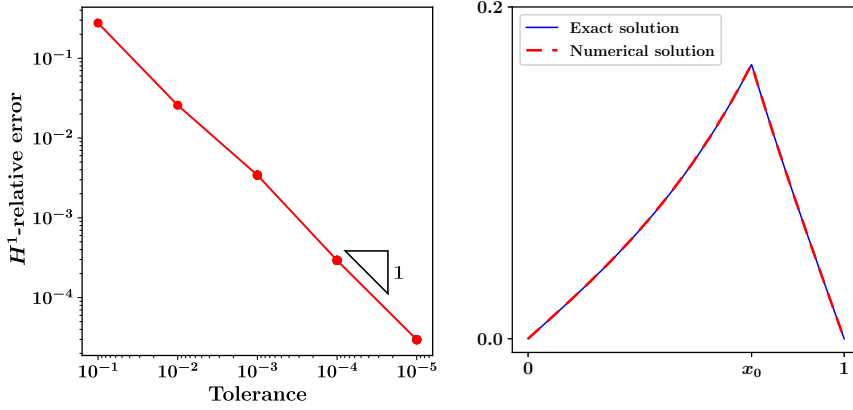


Fig. 6 Left: Relative $\|u - u_{n,h}\|_{H_0^1}$ error v/s tolerance of Algorithm 1. Right: Exact solution of (31) and its adapted numerical approximation using Algorithm 1.

where g is chosen to deliver the exact solution

$$u(x) = -\frac{1}{2\pi} \ln|x - x_0| + |x|^{\frac{2}{3}} \sin\left(\frac{2}{3}(\pi - \arg(x))\right), \quad \arg(x) \in (-\pi, \pi]. \quad (35)$$

The test norm is set to be $\|\cdot\|_V := \|\nabla(\cdot)\|_{L^q(\Omega)}$.

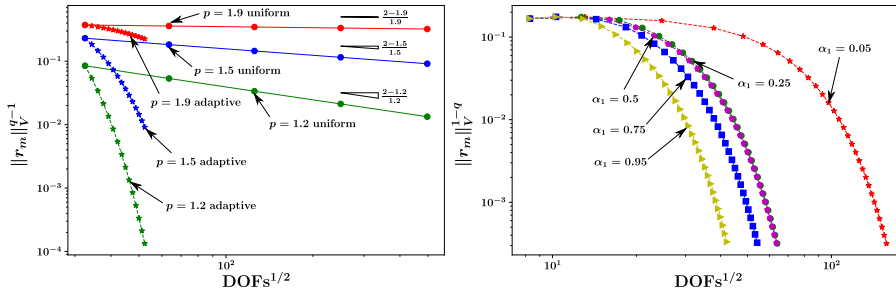


Fig. 7 2D Dirac delta projection. Left: convergence rates of uniform and adaptive h -refinements for several values of p . Right: influence of the choice of the α_1 parameter in Algorithm 1 (the marking criteria).

First, we are going to project the Dirac delta into piecewise polynomial spaces using the compatible pairs provided in sections 4.1 and 4.2, for different parameter settings. In Figure 7 (left) we show convergence rates of the projected Dirac delta using uniform and adaptive h -refinements, computed with the $\mathbb{P}_1/\mathbb{P}_2$ compatible pair, for diverse choices of $p \in (1, 2)$. As in the one dimensional case, we observe that the convergence rates of uniform h -refinements are related with the difference between the regularity exponent $s = 1$ and the critical regularity exponent $s^* = 2/q$ (recall that in 2D we have $W_0^{s,q}(\Omega) \subset \mathcal{C}(\Omega)$ whenever $sq > 2$). The graphical representation is

constructed in terms of the square root of the degrees of freedom (DOFs^{1/2}). In the case of adaptive h -refinements, for each value of p , we present the first 15 iterations of the adaptive algorithm using the marking criteria $\alpha_1 = 0.25$ (see Algorithm 1). Again, exponential convergence is observed due to the fact that the source is localized in only one point. Moreover, in Figure 7 (right), for a fixed value of $p = 1.5$ we show the influence of the choice of the α_1 parameter in the adaptive Algorithm 1. The results were obtained using the $\mathbb{P}_0/(\mathbb{P}_1 + \text{bubbles})$ compatible pair. Observe that the local nature of the source makes it possible to accelerate convergence when $\alpha_1 \rightarrow 1$.

A sequence of meshes obtained from the application of the first step of Algorithm 1 is depicted in Figure 8. Localization of refinements is quite remarkable.

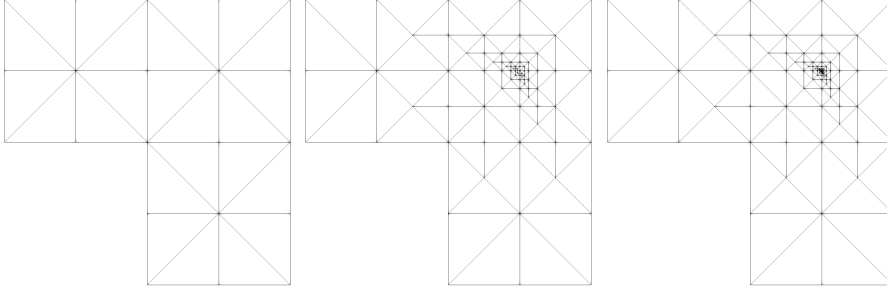


Fig. 8 Adaptive meshes from 2D Dirac delta projection. From left to right: 24, 146, and 218 elements.

Next, we show the performance of the second step of Algorithm 1. We employ the *a posteriori* error estimator given in [15] to catch the L-shape singularity. We should obtain optimal converge rate of order 1 to the exact solution of the *regularized delta problem*. However, as we do not have such a solution in hand, we compute the error using the exact solution (35). Results using $p = 1.2$ and conforming \mathbb{P}_1 piecewise polynomial spaces are depicted in Figure 9. The marking criteria is set to be $\alpha_2 = 0.5$ (see Algorithm 1). The error, and the global *a posteriori* error estimator η_h behave qualitatively the same. The left panel in Figure 9 shows the results obtained using exactly the same L^2 -based *a posteriori* error estimator given in [15]; while the right panel shows the results obtained using the following L^p -version of such estimator:

$$\begin{cases} \eta_h := \left(\sum_{T \in \mathcal{T}_h} \eta_T^p \right)^{\frac{1}{p}}, \\ \eta_T := h_T \|\delta_n + \Delta u_{n,h}\|_{L^p(T)} + \left(\sum_{e \in \partial T} h_e \|\llbracket \partial_{n_e} u_{h,n} \rrbracket_e\|_{L^p(e)}^p \right)^{\frac{1}{p}}, \end{cases}$$

where h_e stands for the diameter of the edge e , and $\llbracket \cdot \rrbracket_e$ denotes the standard *jump* operator on e .

A sequence of meshes obtained from the application of the second step of Algorithm 1 is depicted in Figure 10. Concentration of refinements occurs where is needed.

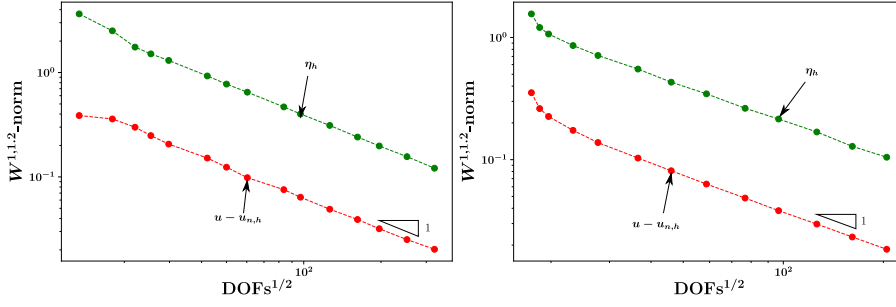


Fig. 9 Convergence of the 2D adaptive regularized PDE (34). Error to the exact solution (red) and *a posteriori* error estimator η_h (green). Left panel: adaptivity driven by L^2 -based *a posteriori* error estimator. Right panel: adaptivity driven by L^p -based *a posteriori* error estimator modification.

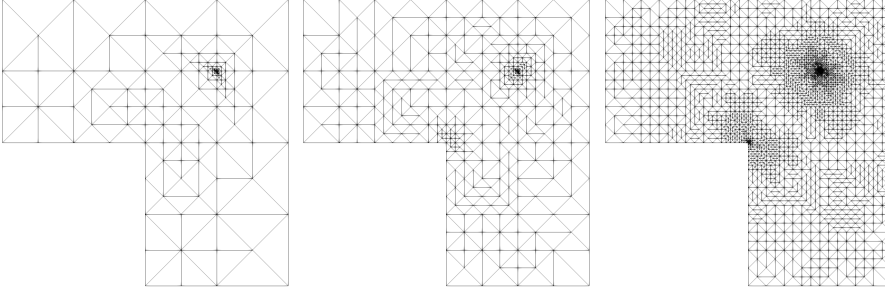


Fig. 10 Adaptive meshes from solving regularized PDE (34). From left to right: 402, 786, and 4646 elements.

5.2 Nonconforming Crouzeix-Raviart elements.

In this subsection we cross the limits of our theory by briefly presenting the performance of nonconforming Crouzeix-Raviart discrete test spaces (see, e.g., [16, Section 10.3], or [29, Section 3.2.3]). The model problem will be the Poisson equation (34), with $\Omega = (0, 1)^2$, $x_0 = (0, 0)$ and $g(x) = -\frac{1}{2\pi} \ln|x|$. The idea will be to obtain a regularized right hand side, in order to approximate the model problem with Crouzeix-Raviart finite elements. Hence, the projected right hand side has to approach the Dirac delta acting on a nonconforming Crouzeix-Raviart space. Of course, the latter is not well defined when x_0 belongs to the border of an element. Hence, we need to define an extension of the Dirac delta functional to cover this situation. To fix ideas, consider a mesh \mathcal{T}_h , and let \mathcal{E}_h^i denote the set of interior edges of the skeleton of \mathcal{T}_h . For any v_h in a Crouzeix-Raviart space linked to mesh \mathcal{T}_h , we consider the following extension of the Dirac delta action:

$$\tilde{\delta}_{x_0}(v_h) := \begin{cases} v_h(x_0) & \text{if } x_0 \in T \in \mathcal{T}_h, \\ \{\!\!\{ v_h \}\!\!\}_e(x_0) & \text{if } x_0 \in e \in \mathcal{E}_h^i, \end{cases}$$

where $\{\!\!\{ \cdot \}\!\!\}_e$ stands for an *average* operator on $e \in \mathcal{E}_h^i$. Using lowest-order Crouzeix-Raviart discrete test spaces, we adaptively project $\tilde{\delta}_{x_0}$ onto a piecewise constants

space \mathbb{P}_0 using the first step of Algorithm 1, with $p = 1.5$ and $\alpha_1 = 0.95$. We use the same *test norm* and *duality map* used in the L-shape computations (see Section 5.1.3). Indeed, the gradient semi-norm becomes a norm in the Crouzeix-Raviart space of vanishing functions at midpoints of edges in $\partial\Omega$.

Finally, with the projected source and its adapted mesh, we directly solve the PDE using lowest-order Crouzeix-Raviart finite elements. The result is (horizontally) depicted in Figure 11.



Fig. 11 Numerical approximation of the Poisson problem in the unit square using nonconforming Crouzeix-Raviart elements, with projected Dirac delta source.

5.3 Line Source

The last experiment is inspired by Example 4. Let $\Omega := (0, 1)^2 \subset \mathbb{R}^2$ be the unit square, and let $\Gamma \in \overline{\Omega}$ be the segment:

$$\Gamma := \{(t, (t - 0.5)^2 + 0.5) \in \mathbb{R}^2 : 0.15 \leq t \leq 0.85\}.$$

We are going to project the linear functional $\ell \in W^{1,q}(\Omega)$ defined by:

$$\ell(v) = \int_{\Gamma} v ds.$$

More generally, ℓ is well-defined, linear and continuous, for any $v \in W^{s,q}(\Omega)$, whenever $sq \geq 1$. Indeed, $v|_{\Gamma} \in W^{s-\frac{1}{q},q}(\Gamma)$. Let $\mathcal{T}_h = \{T_i\}_{i=1}^n$ be a simplicial mesh (not necessarily aligned with Γ), and let us consider the discrete spaces G_h (defined in (23)) and $V_h := \mathbb{P}_1(\mathcal{T}_h) \cap W_0^{1,q}(\Omega) + \mathbb{B}_h(\mathcal{T}_h)$ (see expressions (25) and (26)). In Figure 12, we show convergence rates of the projection of ℓ using uniform and adaptive h -refinements, for several values of p . We observe that the convergence rates of uniform h -refinements are close to the difference between the current regularity exponent $s = 1$ and the critical regularity exponent $s^* = 1/q$ (cf. Remark 9). This graphical representation is constructed in terms of the square root of the degrees of freedom (DOFs^{1/2}). We have observed that adaptive h -refinements practically double the rates of uniform h -refinements. On another hand, Figure 13 shows a sequence of adaptive meshes, obtained for $p = 2, 1.5$ and 1.2 , at a comparable number of degrees of freedom (NDOFs), using the marking criteria parameter $\alpha_1 = 0.4$. As expected, refinements are concentrated along the support of the distribution ℓ , i.e., Γ . We observe better localization of refinements as the value of p decreases.

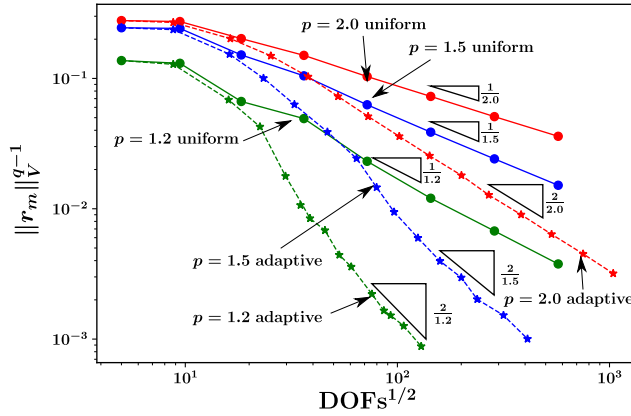


Fig. 12 Line source: convergence rates of uniform and adaptive h -refinements for several values of p .

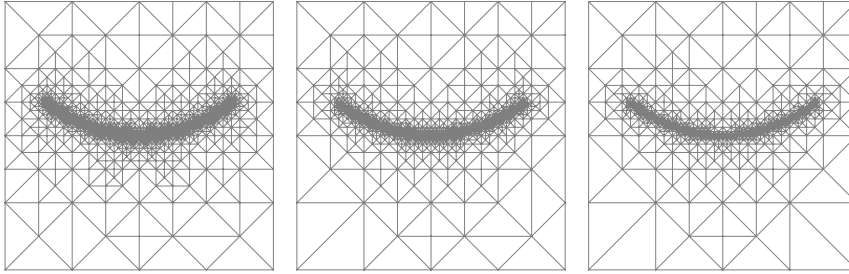


Fig. 13 Line source: Adaptive mesh at a comparable NDOFs, for $p = 2, 1.5$ & 1.2 , respectively.

6 Conclusions

Based on the recent theory of residual minimization in Banach spaces developed in [44], we proposed in this work a method to regularize rough linear functionals, projecting them into piecewise polynomial spaces. The projections has been performed in terms of discrete-dual Banach norms. Particularly, we have studied functionals involving actions over test functions with a certain regularity, i.e., functionals in negative Sobolev spaces. Our approach has two remarkable advantages. First, the regularization can be obtained within low-order piecewise polynomial spaces. Therefore, if such a regularization is used on the right-hand-side of a finite element system, then exact numerical integration can be implemented via Gaussian quadrature formulae. Second, as every residual minimization approach does, the method computes a built-in residual representative, which is proven to be a reliable and efficient *a posteriori* error estimator. Indeed, we have used this estimators to drive adaptive procedures delivering regularized functionals up to any desired precision in the underlying discrete-dual norm. We have observed superior performance of adaptive h -refinements in terms of convergence rates.

On another hand, in terms of the discrete stability of our method, we exhibit two compatible trial-test discrete pairing that can be used in every problem involving rough functionals acting on $W_0^{1,q}(\Omega)$ (see Propositions 8 and 9).

Some future research challenges may include the extension of our theory to nonconforming settings and the regularization of rougher functionals, such as dipole sources in electrostatics [5] or derivatives of Dirac deltas, which appear naturally in high-order PDEs modeling of elastic plates and beams [54].

A Proof of Proposition 8

Through this proof, the symbol \lesssim will denote *less or equal* up to a mesh-independent constant. Recall that we are under the hypothesis of shape-regular simplicial meshes $\mathcal{T}_h = \{T_i\}_{i=1}^n$. Let $\Pi_1 : V \rightarrow \mathbb{P}_1(\mathcal{T}_h)$ be the *Scott-Zhang* interpolation operator (see [29, Section 1.6.2]). For any $T_i \in \mathcal{T}_h$, the restriction $\Pi_1(v)|_{T_i} \in \mathbb{P}_1(T_i)$ satisfies the local estimation

$$\|\Pi_1 v - v\|_{L^q(T_i)} \lesssim h_i \|\nabla v\|_{L^q(\Delta_{T_i})}, \quad \forall v \in V, \quad (36)$$

where $h_i = \text{diam}(T_i)$ and Δ_{T_i} denotes the set of elements in \mathcal{T}_h sharing at least one vertex with T_i (see [29, Lemma 1.130]). Moreover, Π_1 is uniformly bounded with respect to mesh parameters, i.e.,

$$\|\Pi_1 v\|_V \lesssim \|v\|_V, \quad \forall v \in V. \quad (37)$$

For each simplex $T_i \in \mathcal{T}_h$ let $b_i : T_i \rightarrow \mathbb{R}$ be the bubble function defined in (24). Consider now the (Fortin) operator $\Pi : V \mapsto V_m$ locally defined by:

$$\Pi v|_{T_i} := \Pi_1 v|_{T_i} + \alpha_i b_i,$$

where $\alpha_i \in \mathbb{R}$ is chosen such that the following equality holds true:

$$\int_{T_i} \Pi v = \int_{T_i} v, \quad \forall v \in V. \quad (38)$$

Solving for α_i we get:

$$\alpha_i = \left(\int_{T_i} b_i \right)^{-1} \int_{T_i} (v - \Pi_1 v). \quad (39)$$

We will proceed to prove that Π satisfies the Fortin conditions (16) and (17). First, for any $g_n = \sum_{i=1}^n \beta_i \mathcal{G}_i \in G_n$, and any $v \in V$, we have:

$$\langle g_n, \Pi v \rangle_{V^*, V} = \sum_{i=1}^n \beta_i \int_{T_i} \Pi v = \sum_{i=1}^n \beta_i \int_{T_i} v = \langle g_n, v \rangle_{V^*, V}. \quad (\text{by (23) and (46)})$$

Hence, condition (17) is satisfied. To prove (16), let us consider the reference element \hat{T} and the affine mapping $F_i : \hat{T} \rightarrow T_i$ such that $F_i(\hat{x}) = A_i \hat{x} + y_i$. Thus, if $b_{\hat{T}}$ denotes the bubble in \hat{T} , then:

$$b_i(x) = b_{\hat{T}} \circ F_i^{-1}(x), \quad \forall x \in T_i.$$

Moreover, we have the following estimations (see [29, Lemma 1.100]):

$$|\det A_i| = \frac{|T_i|}{|\hat{T}|} \quad \text{and} \quad \|A_i^{-1}\| \leq \frac{h_{\hat{T}}}{\rho_i}$$

where ρ_i is the radius of the largest ball inscribed in T_i and $\|\cdot\|$ is the matrix norm subordinated to the Euclidean norm in \mathbb{R}^d . Notice that $h_{\hat{T}}$ and $|\hat{T}|$ do not depend on the mesh. Using the change-of-variables theorem we get:

$$\int_{T_i} b_i = \int_{\hat{T}} b_{\hat{T}} |\det A_i| = \frac{|T_i|}{|\hat{T}|} \int_{\hat{T}} b_{\hat{T}} = C|T_i|,$$

where $C > 0$ is a mesh independent constant. Hence, we can estimate $|\alpha_i|$ (see (39)) as follows:

$$|\alpha_i| \lesssim \frac{1}{|T_i|} \|v - \Pi_1 v\|_{L^q(T_i)} |T_i|^{\frac{1}{p}} = \frac{1}{|T_i|^{\frac{1}{q}}} \|v - \Pi_1 v\|_{L^q(T_i)} \lesssim \frac{h_i}{|T_i|^{\frac{1}{q}}} \|\nabla v\|_{L^q(\Delta_{T_i})}, \quad (40)$$

where we have used (36) in the last inequality. Additionally, we estimate the bubble function semi-norm by the following classical result (see [29, Lemma 1.101]):

$$\|\nabla b_i\|_{L^q(T_i)} \lesssim \|A_i^{-1}\| |\det A_i|^{\frac{1}{q}} \|\nabla b_{\hat{T}}\|_{L^q(\hat{T})} \lesssim \frac{|T_i|^{\frac{1}{q}}}{\rho_i}. \quad (41)$$

Combining (40) and (41) we get:

$$|\alpha_i| \|\nabla b_{T_i}\|_{L^q(T_i)} \lesssim \frac{h_i}{\rho_i} \|\nabla v\|_{L^q(\Delta_{T_i})} \lesssim \|\nabla v\|_{L^q(\Delta_{T_i})}, \quad (42)$$

where the last inequality holds true because of the shape-regularity of the mesh. Shape-regularity also implies that each element of the mesh is contained in a uniformly bounded (say, $M \in \mathbb{N}$) number of sets like Δ_{T_i} . Finally, (16) holds true since

$$\begin{aligned} \|\nabla \Pi v\|_{L^q(\Omega)}^q &= \sum_{i=1}^n \|\nabla \Pi v\|_{L^q(T_i)}^q \leq 2^{q-1} \sum_{i=1}^n \left(\|\nabla \Pi_1 v\|_{L^q(T_i)}^q + |\alpha_i|^q \|\nabla b_i\|_{L^q(T_i)}^q \right) \\ &\lesssim \|\nabla \Pi_1 v\|_{L^q(\Omega)}^q + M \sum_{i=1}^n \|\nabla v\|_{L^q(T_i)}^q \lesssim \|\nabla v\|_{L^q(\Omega)}^q, \end{aligned}$$

where we have used Hölder inequality, together with (37) and (42).

B Proof of Proposition 9

Again, through this proof, the symbol \lesssim will denote *less or equal* up to a mesh-independent constant. The proof of Proposition 9 requires the following previous lemma.

Lemma 2 *Under the hypothesis of Assumption 1, let $\{\varphi_i\}_{i=1}^{N_v}$ be the set of nodal basis functions spanning $\mathbb{P}_1(\mathcal{T}_h) \cap W_0^{1,p}(\Omega)$. There exists a (bi-orthogonal) set $\{\psi_i\}_{i=1}^{N_v} \subset \mathbb{P}_2(\mathcal{T}_h) \cap W_0^{1,q}(\Omega)$ such that:*

$$\int_{\Omega} \varphi_i \psi_j = \eta_i \delta_{ij}, \quad \forall i, j = 1, \dots, N_v, \quad (43)$$

where δ_{ij} denotes the Kronecker delta, and η_i denotes the scaling constant of the patch $P_i = \overline{\text{supp } \varphi_i}$ (see Assumption 1). Moreover we have the estimate:

$$\|\nabla \psi_i\|_{L^q(\Omega)} \lesssim \frac{\eta_i^{\frac{1}{q}}}{\min_{T \in P_i} \rho_T}, \quad \forall i = 1, \dots, N_v, \quad (44)$$

where ρ_T denotes the diameter of the largest ball that can be inscribed in T .

Proof. By Assumption 1, the patch P_i supporting the nodal basis function φ_i has a reference patch \widehat{P}_i , having the same configuration of elements of P_i . Hence, the patch \widehat{P}_i has a single interior vertex denoted by x_0 . Each other vertex of this patch is linked to x_0 through a unique interior edge. Let n_e be the number of exterior vertices of the patch \widehat{P}_i (equivalently, the set of interior edges of the patch \widehat{P}_i). The local \mathbb{P}_1 trial basis functions for this reference patch will consist in $n_e + 1$ shape functions $\{\widehat{\varphi}_j\}_{j=0}^{n_e}$, where $\widehat{\varphi}_0$ denotes the trial function associated with the interior vertex x_0 . We want to construct a \mathbb{P}_2 test function $\widehat{\psi}_i$, supported on the patch \widehat{P}_i , such that:

$$\int_{\widehat{P}_i} \widehat{\varphi}_j \widehat{\psi}_i = \delta_{0j}, \quad \forall j = 0, 1, \dots, n_e. \quad (45)$$

We provide a two-dimensional procedure to construct such a $\widehat{\psi}_i$, which can be easily extended to three dimensions. Let us denote by $\{\widehat{T}_1, \dots, \widehat{T}_{n_e}\}$ the set of simplicial elements that make up the patch \widehat{P}_i , and let $\{x_1, \dots, x_{n_e}\}$ be the set of exterior vertices of the patch \widehat{P}_i , enumerated so that $\widehat{T}_1 = \text{conv}(x_0, x_1, x_2)$, $\widehat{T}_2 = \text{conv}(x_0, x_2, x_3)$, \dots , $\widehat{T}_{n_e} = \text{conv}(x_0, x_{n_e}, x_1)$. Consider a reference simplex $S := \{(s, t) \in \mathbb{R}^2 : s \in [0, 1], t \in [0, s]\}$ and observe that each element \widehat{T}_j can be obtained from S through the affine transformation $(s, t) \mapsto x_0 + s(x_j - x_0) + t(x_{j+1} - x_j)$ whose Jacobian is constant (we are using the logical convention $x_{n_e+1} = x_1$). The shape functions $\widehat{\varphi}_0$, $\widehat{\varphi}_j$ and $\widehat{\varphi}_{j+1}$, restricted to the element \widehat{T}_j , are such that:

$$\begin{aligned} \widehat{\varphi}_0(x_0 + s(x_j - x_0) + t(x_{j+1} - x_j)) &= 1 - s, \\ \widehat{\varphi}_j(x_0 + s(x_j - x_0) + t(x_{j+1} - x_j)) &= s - t, \\ \widehat{\varphi}_{j+1}(x_0 + s(x_j - x_0) + t(x_{j+1} - x_j)) &= t, \end{aligned}$$

for all $(s, t) \in S$. For a given constant $\kappa \neq 0$ (to be determined later), we propose the following construction of $\widehat{\psi}_i$ restricted to the element \widehat{T}_j :

$$\widehat{\psi}_i \Big|_{\widehat{T}_j} (x_0 + s(x_j - x_0) + t(x_{j+1} - x_j)) = \kappa(s-1)(5s-3), \quad \forall (s, t) \in S.$$

Observe that $\widehat{\psi}_i$ is invariant with respect to the parameter t , and that $\widehat{\psi}_i$ vanishes when restricted to the exterior edge $\text{conv}(x_j, x_{j+1})$, i.e., when $s = 1$. Moreover, this construction is continuous across interior edges $\text{conv}(x_0, x_j) = \widehat{T}_j \cap \widehat{T}_{j-1}$. Indeed,

$$\begin{aligned} \widehat{\psi}_i \Big|_{\widehat{T}_j} (x_0 + s(x_j - x_0) + 0(x_{j+1} - x_j)) &= \kappa(s-1)(5s-3), & (\text{since } t = 0) \\ \widehat{\psi}_i \Big|_{\widehat{T}_{j-1}} (x_0 + s(x_{j-1} - x_0) + s(x_j - x_{j-1})) &= \kappa(s-1)(5s-3). & (\text{since } t = s) \end{aligned}$$

Furthermore, $\widehat{\psi}_i$ is element-wise orthogonal to the shape functions $\{\widehat{\varphi}_1, \dots, \widehat{\varphi}_{n_e}\}$. Indeed,

$$\begin{aligned} \int_{\widehat{T}_j} \widehat{\varphi}_j \widehat{\psi}_i &= |\widehat{T}_j| \frac{\kappa}{2} \int_0^1 \int_0^s (s-t)(s-1)(5s-3) dt ds = |\widehat{T}_j| \frac{\kappa}{4} \int_0^1 s^2 (s-1)(5s-3) ds, \\ \int_{\widehat{T}_j} \widehat{\varphi}_{j+1} \widehat{\psi}_i &= |\widehat{T}_j| \frac{\kappa}{2} \int_0^1 \int_0^s t(s-1)(5s-3) dt ds = |\widehat{T}_j| \frac{\kappa}{4} \int_0^1 s^2 (s-1)(5s-3) ds, \end{aligned}$$

where it is easy to see that the integral on the right-hand-side vanishes. Finally, we observe that the integral $\int_{\widehat{T}_j} \widehat{\varphi}_0 \widehat{\psi}_i$ do not vanish. So we can adjust the constant $\kappa \neq 0$ to get $\int_{\widehat{P}_i} \widehat{\varphi}_0 \widehat{\psi}_i = 1$, as desired.

Now, for each element $T \subset P_i$ define $\psi_i|_T = \widehat{\psi}_i \circ F_T^{-1}$ (see Assumption 1) and take a nodal trial function φ_j . If the support of φ_j does not intersect P_i , then $\int_{\Omega} \varphi_j \psi_i = 0$. Otherwise, there must be $j^* \in \{0, 1, \dots, n_e\}$ such that $\varphi_j|_T = \widehat{\varphi}_{j^*} \circ F_T^{-1}$, for all $T \subset P_i$. In that case, using the change-of-variables theorem and equation (30), we have:

$$\int_{\Omega} \varphi_j \psi_i = \sum_{T \subset P_i} \int_T \varphi_j \psi_i = \sum_{\widehat{T} \subset \widehat{P}_i} \int_{\widehat{T}} \widehat{\varphi}_{j^*} \widehat{\psi}_i \frac{|T|}{|\widehat{T}|} = \eta_i \int_{\widehat{P}_i} \widehat{\varphi}_{j^*} \widehat{\psi}_i = \eta_i \delta_{0j^*} = \eta_i \delta_{ij},$$

since the case $j^* = 0$ occurs exactly when $j = i$.

To estimate the norm of ψ_i , first observe that for each element $T \subset P_i$:

$$\|\nabla \psi_i\|_{L^q(T)} \lesssim \|A_T^{-1}\| \|\det A_T\|^{\frac{1}{q}} \|\nabla \widetilde{\psi}_i\|_{L^q(\widehat{T})} \lesssim \frac{\eta_i^{\frac{1}{q}}}{\min_{T \in P_i} \rho_T} \|\nabla \widetilde{\psi}_i\|_{L^q(\widehat{T})}.$$

Hence,

$$\|\nabla \psi_i\|_{L^q(P_i)}^q = \sum_{T \subset P_i} \|\nabla \psi_i\|_{L^q(T)}^q \lesssim \frac{\eta_i}{\min_{T \in P_i} \rho_T^q} \sum_{\widehat{T} \subset \widehat{P}_i} \|\nabla \widetilde{\psi}_i\|_{L^q(\widehat{T})}^q = \frac{\eta_i}{\min_{T \in P_i} \rho_T^q} \|\nabla \widetilde{\psi}_i\|_{L^q(\widehat{P}_i)}^q,$$

which leads to estimate (44). \square

Now, let us prove Proposition 9. Recall that we are under the hypothesis that $\mathcal{T}_h = \{T_i\}_{i=1}^n$ corresponds to a family of shape-regular simplicial meshes. Let $\Pi_1 : V \rightarrow \mathbb{P}_1(\mathcal{T}_h)$ be the *Scott-Zhang* interpolation operator, satisfying (for any $T_i \in \mathcal{T}_h$)

the local estimation (36), together with the global boundedness property (37). Consider the (Fortin) operator $\Pi : V \mapsto V_m$ defined by:

$$\Pi v := \Pi_1 v + \sum_{j=1}^{N_v} \alpha_j \psi_j,$$

where $\psi_j \in \mathbb{P}_2(\mathcal{T}_h)$ satisfies (43) and $\alpha_j \in \mathbb{R}$ is chosen such that the following equality holds true:

$$\int_{\Omega} \varphi_i \Pi v = \int_{\Omega} \varphi_i v, \quad \forall v \in V, \quad \forall i = 1, \dots, N_v. \quad (46)$$

Solving for α_i we get

$$\alpha_i = \frac{1}{\eta_i} \int_{\Omega} \varphi_i (v - \Pi_1 v). \quad (47)$$

Observe that (46) implies property (17) of the Fortin operator. To prove property (16) we start estimating α_i . So let $P_i := \overline{\text{supp}} \varphi_i$ be the patch of simplices supporting the nodal basis function φ_i . We have:

$$|\alpha_i| \leq \frac{1}{\eta_i} \sum_{T \in P_i} \|\varphi_i\|_{L^p(T)} \|v - \Pi_1 v\|_{L^q(T)} \lesssim \sum_{T \in P_i} \frac{|T|^{\frac{1}{p}}}{\eta_i} h_T \|\nabla v\|_{L^q(\Delta_T)} \lesssim \frac{h_i}{\eta_i} |P_i|^{\frac{1}{p}} C_i(v),$$

where $h_i = \max_{T \in P_i} h_T$, while Δ_T is the subset of \mathcal{T}_h containing all the elements sharing at least one vertex with T , and

$$C_i(v) := \left(\sum_{T \in P_i} \|\nabla v\|_{L^q(\Delta_T)}^q \right)^{\frac{1}{q}}.$$

Let $\tilde{T} \subset P_i$ such that $\rho_{\tilde{T}} = \min_{T \in P_i} \rho_T$. By quasi-uniformity of the patches, there is a mesh-independent constant $c > 0$, such that $h_i \leq c h_{\tilde{T}}$. Hence, by shape-regularity we have that $h_i / \rho_{\tilde{T}} \lesssim h_{\tilde{T}} / \rho_{\tilde{T}}$ is uniformly bounded from above. Next, using the estimate (44) we get:

$$|\alpha_i| \|\nabla \psi_i\|_{L^q(P_i)} \lesssim \frac{|P_i|^{\frac{1}{p}}}{\eta_i^{\frac{1}{p}}} \frac{h_i}{\rho_{\tilde{T}}} C_i(v) \lesssim \left(\sum_{T \subset P_i} \frac{|T|}{\eta_i} \right)^{\frac{1}{p}} C_i(v) = |\hat{P}_i|^{\frac{1}{p}} C_i(v).$$

By shape-regularity, each element T of the mesh, is contained in an uniformly bounded (say, $M \in \mathbb{N}$) number of macro-patches like Δ_T . This leads to the estimate:

$$\sum_{i=1}^{N_v} |\alpha_i|^q \|\nabla \psi_i\|_{L^q(P_i)}^q \lesssim \sum_{i=1}^{N_v} \sum_{T \in P_i} \|\nabla v\|_{L^q(\Delta_T)}^q \leq (d+1)M \|\nabla v\|_{L^q(\Omega)}^q. \quad (48)$$

Finally, we have:

$$\begin{aligned} \|\nabla \Pi v\|_{L^q(\Omega)}^q &= \sum_{T \in \mathcal{T}_h} \left\| \nabla \Pi_1 v + \sum_{\{i/T \subset P_i\}} \alpha_i \nabla \psi_i \right\|_{L^q(T)}^q \\ &\leq (d+2)^{q-1} \sum_{T \in \mathcal{T}_h} \left(\|\nabla \Pi_1 v\|_{L^q(T)}^q + \sum_{\{i/T \subset P_i\}} |\alpha_i|^q \|\nabla \psi_i\|_{L^q(T)}^q \right) \\ &\lesssim \|\nabla \Pi_1 v\|_{L^q(\Omega)}^q + \sum_{i=1}^{N_i} |\alpha_i|^q \|\nabla \psi_i\|_{L^q(P_i)}^q \lesssim \|\nabla v\|_{L^q(\Omega)}^q. \end{aligned}$$

Acknowledgements

The authors want to thank Diego Paredes for helping with preliminary numerical experiments, Michael Karkulik for his pertinent advice, and also want to thank the unknown reviewers for their insightful suggestions.

The work by IM and FM was done in the framework of Chilean FONDECYT research project #1160774. The work of SR was supported by the Chilean grant ANID Fondecyt 3210009. IM and SR have also received funding from the European Union's Horizon 2020 research and innovation programme under the Marie Skłodowska-Curie grant agreement No 777778 (MATHROCKS). The research by KvdZ was supported by the Engineering and Physical Sciences Research Council (EPSRC) under grant EP/T005157/1. IM acknowledges support from the project DI Investigación Innovadora Interdisciplinaria PUCV No 039.409/2021, and project DI PUCV No 039.375/2021.

References

1. Adams, R., Fournier, J.: Sobolev spaces, vol. 140. Academic press (2003)
2. Agnelli, J.P., Garau, E., Morin, P.: A posteriori error estimates for elliptic problems with Dirac measure terms in weighted spaces. *ESAIM Math. Model. Numer. Anal.* **48**(6), 1557–1581 (2014)
3. Allendes, A., Otárola, E., Salgado, A.: A posteriori error estimates for the Stokes problem with singular sources. *Comput. Methods Appl. Mech. Engrg.* **345**, 1007–1032 (2018)
4. Allendes, A., Otárola, E., Salgado, A.: A posteriori error estimates for the stationary Navier-Stokes equations with Dirac measures. *SIAM J. Sci. Comput.* **42**(3), A1860–A1884 (2020)
5. Alonso-Rodríguez, A., Camaño, J., Rodríguez, R., Valli, A.: A posteriori error estimates for the problem of electrostatics with a dipole source. *Comput. Math. Appl.* **68**, 464–485 (2014)
6. Apel, T., Benedix, O., Sirch, D., Vexler, B.: A priori mesh grading for an elliptic problem with Dirac right-hand side. *SIAM J. Numer. Anal.* **49**(3), 992–1005 (2011)
7. Araya, R., Behrens, E., Rodríguez, R.: A posteriori error estimates for elliptic problems with Dirac delta source terms. *Numer. Math.* **105**(2), 193–216 (2006)
8. Araya, R., Behrens, E., Rodríguez, R.: An adaptive stabilized finite element scheme for a water quality model. *Comput. Methods Appl. Math.* **196**(29), 2800–2812 (2007)
9. Babuška, I.: Error-bounds for finite element method. *Numer. Math.* **16**(4), 322–333 (1971)
10. Bencomo, M., Symes, W.: Discretization of multipole sources in a finite difference setting for wave propagation problems. *J. Comput. Phys.* **386**, 296–322 (2019)
11. Benvenuti, E., Ventura, G., Ponara, N., Tralli, A.: Accuracy of three-dimensional analysis of regularized singularities. *Int. J. Numer. Meth. Engrg.* **101**, 29–53 (2014)
12. Binev, P., Dahmen, W., De Vore, R.: Adaptive finite element methods with convergence rates. *Numer. Math.* **97**, 219–268 (2004)

13. Blechta, J., Málek, J., Vohralík, M.: Localization of the $W^{-1,q}$ norm for local a posteriori efficiency. *IMA J. Numer. Anal.* **40**, 914–950 (2020)
14. Boffi, D., Brezzi, F., Fortin, M., et al.: Mixed finite element methods and applications, vol. 44, Springer Series in Computational Mathematics. Springer (2013)
15. Bonito, A., DeVore, R.A., Nochetto, R.: Adaptive finite element methods for elliptic problems with discontinuous coefficients. *SIAM J. Numer. Anal.* **51**, 3106–3134 (2013)
16. Brenner, S., Scott, L.R.: The Mathematical Theory of Finite Element Methods, vol. 15, Texts in Applied Mathematics. Springer (2008)
17. Brezis, H.: Functional analysis, Sobolev spaces and partial differential equations. Springer (2010)
18. Casado-Díaz, J., Rebollo, T.C., Girault, V., Mármol, M.G., Murat, F.: Finite elements approximation of second order linear elliptic equations in divergence form with right-hand side in l^1 . *Numer. Math.* **105**(3), 337–374 (2007)
19. Cascon, J.M., H., N.R.: Quasioptimal cardinality of AFEM driven by nonresidual estimators. *IMA J. Numer. Anal.* **46**(5), 2524–2550 (2011)
20. Cascon, J.M., Kreuzer, C., Nochetto, R.H., Siebert, K.G.: Quasi-optimal convergence rate for an adaptive finite element method. *SIAM J. Numer. Anal.* **46**(5), 2524–2550 (2008)
21. Cioranescu, I.: Geometry of Banach spaces, duality mappings and nonlinear problems, vol. 62, Mathematics and Its Applications. Kluwer Academic Publishers (1990)
22. Clain, S.: Finite element approximations for the Laplace operator with a right-hand side measure. *Math. Models Methods Appl. Sci.* **6**, 713–719 (1995)
23. Cohen, A., DeVore, R., Nochetto, R.: Convergence rates of AFEM with H^{-1} data. *Found. Comput. Math.* **12**, 671–718 (2012)
24. D’angelo, C.: Finite element approximation of elliptic problems with Dirac measure terms in weighted spaces: Applications to one-and three-dimensional coupled problems. *SIAM J. Numer. Anal.* **50**(1), 194–215 (2012)
25. Demkowicz, L., Gopalakrishnan, J.: An overview of the discontinuous Petrov–Galerkin method. In: X. Feng, O. Karakashian, Y. Xing (eds.) Recent Developments in Discontinuous Galerkin Finite Element Methods for Partial Differential Equations: 2012 John H Barrett Memorial Lectures, *The IMA Volumes in Mathematics and its Applications*, vol. 157, pp. 149–180. Springer, Cham (2014)
26. Di Nezza, E., Palatucci, G., Valdinoci, E.: Hitchhiker’s guide to the fractional Sobolev spaces. *Bull. Sci. math.* **136**, 521–573 (2012)
27. Dörfler, W.: A convergent adaptive algorithm for Poisson’s equation. *SIAM J. Numer. Anal.* **33**, 1106–1124 (1996)
28. Eriksson, K.: Improved accuracy by adapted mesh-refinements in the finite element method. *Math. Comp.* **44**(170), 321–343 (1985)
29. Ern, A., Guermond, J.: Theory and practice of finite elements, vol. 159, Applied Mathematical Sciences. Springer (2013)
30. Ern, A., Guermond, J.: Finite Elements I: Approximation and Interpolation, vol. 72, Texts in Applied Mathematics. Springer (2021)
31. Ern, A., Guermond, J.L.: A converse to Fortin’s Lemma in Banach spaces. *C. R. Math. Acad. Sci. Paris* **354**, 1092–1095 (2016)
32. Führer, T., Heuer, N., Karkulik, M.: MINRES for second-order PDEs with singular data. arXiv:2111.00103v1 [math.NA] (2021)
33. Fuica, F., Lepe, F., Otárola, E., Quero, D.: A posteriori error estimates in $W^{1,p} \times L^p$ spaces for the Stokes system with Dirac measures. *Comput. Math. Appl.* **94**, 47–59 (2021)
34. Gallouët, T., Herbin, R.: Convergence of linear finite elements for diffusion equations with measure data. *C. R. Math. Acad. Sci. Paris* **338**, 81–84 (2004)
35. Gaspoz, F.D., Morin, P., Veeger, A.: A posteriori error estimates with point sources in fractional Sobolev spaces. *Numer. Methods Partial Differential Equations* **33**(4), 1018–1042 (2017)
36. Gjerde, I.G., Kumar, K., Nordbotten, J.M., Wohlmuth, B.: Splitting method for elliptic equations with line sources. *ESAIM Math. Model. Numer. Anal.* **53**(5), 1715–1739 (2019)
37. Gopalakrishnan, J., Qiu, W.: An analysis of the practical DPG method. *Math. Comp.* **83**, 537–552 (2014)
38. Heltai, L., Lei, W.: A priori error estimates of regularized elliptic problems. *Numer. Math.* **146**, 571–596 (2020)
39. Hosseini, B., Nigam, N., Stockie, J.: On regularizations of the Dirac delta distribution. *J. Comput. Phys.* **305**, 423–447 (2016)
40. Li, H., Wan, X., Yin, P., Zhao, L.: Regularity and finite element approximation for two-dimensional elliptic equations with line Dirac sources. *J. Comput. Appl. Math.* **393**, 113,518 (2021)

41. Morin, P., Nochetto, R., Siebert, K.: Data oscillation and convergence of adaptive FEM. *SIAM J. Numer. Anal.* **38**, 466–488 (2000)
42. Muga, I., Tyler, M.J.W., van der Zee, K.G.: The Discrete-Dual Minimal-Residual Method (DDMRes) for Weak Advection-Reaction Problems in Banach Spaces. *Comput. Methods Appl. Math.* **19**(3), 557–579 (2019)
43. Muga, I., van der Zee, K.G.: Discretization of linear problems in Banach spaces: Residual minimization, nonlinear Petrov-Galerkin, and monotone mixed methods. arXiv:1511.04400v3 [math.NA] (2018)
44. Muga, I., Van der Zee, K.G.: Discretization of linear problems in Banach spaces: Residual minimization, nonlinear Petrov-Galerkin, and monotone mixed methods. *SIAM J. Numer. Anal.* **58**(6), 3406–3426 (2020)
45. Nochetto, R.: Pointwise a posteriori error estimates for elliptic problems on highly graded meshes. *Math. Comp.* **64**, 1–22 (1995)
46. Scott, R.: Finite element convergence for singular data. *Numer. Math.* **21**(4), 317–327 (1973)
47. Stakgold, I., Holst, M.: *Green's Functions and Boundary Value Problems*, vol. 99, Pure and Applied Mathematics. John Wiley & Sons (2011)
48. Stevenson, R.: Optimality of a standard adaptive finite element method. *Found. Comput. Math.* **7**(2), 245–269 (2007)
49. Stevenson, R.P.: An optimal adaptive finite element method. *SIAM J. Numer. Anal.* **42**(5), 2188–2217 (2005)
50. Suarez, J.P., Jacobs, J.B., Don, W.S.: A high-order Dirac-delta regularization with optimal scaling in the spectral solution of one-dimensional singular hyperbolic conservation laws. *SIAM J. Sci. Comput.* **36**(4), A1831–A1849 (2014)
51. Tornberg, A., Engquist, B.: Numerical approximations of singular source terms in differential equations. *J. Comput. Phys.* **200**(2), 462–488 (2004)
52. Verfürth, R.: *A Review of A Posteriori Error Estimation and Adaptive Mesh-Refinement Techniques*. Wiley-Teubner series advances in numerical mathematics (1996)
53. Waldén, J.: On the approximation of singular source terms in differential equations. *Numer. Methods Partial Differential Equations* **15**(4), 503–520 (1999)
54. Yavari, A., Sarkani, S., Moyer, E.: On applications of generalized functions to beam bending problems. *Int. J. Solids Struct.* **37**, 5675–5705 (2000)